Limited effect of anthropogenic nitrogen oxides on secondary organic aerosol formation

Y. Zheng, N. Unger, A. Hodzic, L. Emmons, Christoph Knote, S. Tilmes, J.-F. Lamarque, P. Yu

Angaben zur Veröffentlichung / Publication details:

Zheng, Y., N. Unger, A. Hodzic, L. Emmons, Christoph Knote, S. Tilmes, J.-F. Lamarque, and P. Yu. 2015. "Limited effect of anthropogenic nitrogen oxides on secondary organic aerosol formation." *Atmospheric Chemistry and Physics* 15 (23): 13487–506. https://doi.org/10.5194/acp-15-13487-2015.

Atmos. Chem. Phys., 15, 13487–13506, 2015
www.atmos-chem-phys.net/15/13487/2015/
doi:10.5194/acp-15-13487-2015

Atmospheric Chemistry and Physics Open Access EGU

Limited effect of anthropogenic nitrogen oxides on secondary organic aerosol formation

Y. Zheng[1], N. Unger[1,2], A. Hodzic[3], L. Emmons[3], C. Knote[3,a], S. Tilmes[3], J.-F. Lamarque[3], and P. Yu[4,5,b]

[1]Department of Geology and Geophysics, Yale University, New Haven, CT, USA
[2]School of Forestry and Environmental Studies, Yale University, New Haven, CT, USA
[3]Atmospheric Chemistry Observations and Modeling Laboratory, National Center for Atmospheric Research, Boulder, CO, USA
[4]Department of Atmospheric and Oceanic Sciences, University of Colorado, Boulder, CO, USA
[5]Laboratory for Atmospheric and Space Physics, University of Colorado, Boulder, CO, USA
[a]now at: Meteorologisches Institut, Ludwig-Maximilians-Universitaet, Munich, Germany
[b]now at: Earth System Research Laboratory, National Oceanic and Atmospheric Administration, Boulder, CO, USA

Correspondence to: Y. Zheng (yiqi.zheng@yale.edu)

Received: 21 July 2015 – Published in Atmos. Chem. Phys. Discuss.: 28 August 2015
Revised: 7 November 2015 – Accepted: 23 November 2015 – Published: 8 December 2015

Abstract. Globally, secondary organic aerosol (SOA) is mostly formed from emissions of biogenic volatile organic compounds (VOCs) by vegetation, but it can be modified by human activities as demonstrated in recent research. Specifically, nitrogen oxides ($NO_x = NO + NO_2$) have been shown to play a critical role in the chemical formation of low volatility compounds. We have updated the SOA scheme in the global NCAR (National Center for Atmospheric Research) Community Atmospheric Model version 4 with chemistry (CAM4-chem) by implementing a 4-product volatility basis set (VBS) scheme, including NO_x-dependent SOA yields and aging parameterizations. Small differences are found for the no-aging VBS and 2-product schemes; large increases in SOA production and the SOA-to-OA ratio are found for the aging scheme. The predicted organic aerosol amounts capture both the magnitude and distribution of US surface annual mean measurements from the Interagency Monitoring of Protected Visual Environments (IMPROVE) network by 50 %, and the simulated vertical profiles are within a factor of 2 compared to aerosol mass spectrometer (AMS) measurements from 13 aircraft-based field campaigns across different regions and seasons. We then perform sensitivity experiments to examine how the SOA loading responds to a 50 % reduction in anthropogenic nitric oxide (NO) emissions in different regions. We find limited SOA reductions of 0.9–5.6, 6.4–12.0 and 0.9–2.8 % for global, southeast US and Amazon NO_x perturbations, respectively. The fact that SOA formation is almost unaffected by changes in NO_x can be largely attributed to a limited shift in chemical regime, to buffering in chemical pathways (low- and high-NO_x pathways, O_3 versus NO_3-initiated oxidation) and to offsetting tendencies in the biogenic versus anthropogenic SOA responses.

1 Introduction

Organic aerosols (OAs) account for a substantial fraction of atmospheric fine particulate matter and can have significant impacts on both air quality (Huang et al., 2014; Zhang et al., 2007) and climate (Carslaw et al., 2010). Previous research suggests that organic compounds make up between 10 and 90 % of the total aerosol mass at continental mid-latitudes and in tropical forests (Andreae and Crutzen, 1997; Kanakidou et al., 2005; Putaud et al., 2010; Seinfeld and Pankow, 2003). Aside from primary organic aerosols (POAs) that are directly emitted into the atmosphere, another major fraction of OA is composed of secondary organic aerosols (SOAs), which are formed through chemical transformation of anthropogenic and biogenic volatile organic compounds (AVOCs and BVOCs). AVOCs include aromatics, alkanes and alkenes of about 25, 44 and 38 TgC $year^{-1}$, respec-

tively, from industrial processes, fossil fuel use, biomass burning and road vehicles (Williams and Koppmann, 2007). Isoprene and monoterpenes are the dominant BVOC emissions with estimated global source strengths of about 500 and 150 TgC $year^{-1}$, respectively (Guenther et al., 2012). POA can also re-evaporate upon dilution and participate in the chemical oxidation processes leading to the formation of SOA (Robinson et al., 2007).

Biogenic SOA (BSOA) is usually regarded as natural aerosol and as such cannot be addressed by emission control legislation. Recent research implied that anthropogenic compounds facilitate BSOA formation, thus providing the possibility to control BSOA by regulating the emission of other precursor pollutants like AVOCs, POA and nitrogen oxides (Carlton et al., 2010; Emanuelsson et al., 2013; Hoyle et al., 2011; Lin et al., 2013; Rollins et al., 2012; Volkamer et al., 2006). For example, Carlton et al. (2010) have shown that, in the southeast US, up to 50 % of the total BSOA surface atmospheric loading is attributed to controllable pollution emissions. Spracklen et al. (2011) found that at the global scale the model with a large human-interfered SOA source was the most consistent with observations, which includes a maximum of 10 % SOA (10 Tg $year^{-1}$) from fossil sources, and the extra is mostly likely due to an anthropogenic pollution enhancement of BSOA. The potential impacts of human activities are visible in every step of BSOA formation: the amount of naturally emitted BVOCs through land use and land cover change, the oxidative transformation of BVOCs to semivolatiles through altering atmospheric oxidant concentrations, and the partitioning behavior to the aerosol phase through modifying the load and miscibility of pre-existing organic aerosol (Hoyle et al., 2011).

Among the multiple human-induced influences, nitrogen oxides ($NO_x = NO + NO_2$, emitted from many fossil-fuel driven activity sectors) play a critical role in SOA formation through several aspects. First, through the competitive chemistry of organo-peroxy radicals (RO_2) formed from oxidation of AVOC and BVOC precursors, which can react mainly with NO at high NO_x or hydroperoxyl (HO_2) and peroxy radicals (RO_2) at low NO_x conditions (Kroll and Seinfeld, 2008; Ziemann and Atkinson, 2012). Calculating the SOA yield dependence on NO_x is challenging because the OH / O_3 ratio depends on the VOC / NO_x ratio (Presto et al., 2005). Lane et al. (2008) suggested that SOA yields could be calculated by a linear combination of the "pure" mass yields scaled by the strength of each branch. In many SOA models (e.g., Heald et al., 2008; Lane et al., 2008; Pye et al., 2010), the representative reactions for each branch are

$$\text{low} - NO_x \text{ condition} : RO_2 + HO_2 \rightarrow \text{ROOH},$$
$$\text{high} - NO_x \text{ condition} : RO_2 + NO \rightarrow RONO_2.$$

For AVOCs like light aromatics (Ng et al., 2007) and BVOCs like isoprene (Kroll et al., 2006) and monoterpenes (Presto et al., 2005), both the ROOH groups and the $RONO_2$ groups can be low in volatility thus facilitating SOA formation, but $RONO_2$ is not the dominant product of the $RO_2 + NO$ channel; therefore, the high-NO_x pathway usually has lower yields of SOA. Second, NO_x can influence SOA formation through nighttime nitrate radical (NO_3) chemistry. This pathway has a distinctive chemical signature due to the high yields of organic nitrate ($RONO_2$), which also forms during daytime photooxidation in the presence of NO but with a lower yield. The importance of NO_3-initiated SOA formation has been confirmed by chamber experiments (Griffin et al., 1999; Ng et al., 2008) and field studies, e.g., in Bakersfield, California, NO_3 chemistry contributed approximately a third of the nighttime increase in total OA (Rollins et al., 2012). Finally, NO_x levels can impact the atmospheric oxidation capacity. In the NO_x-limited regime (in terms of O_3 formation), the OH-initiated oxidation of CO, methane (CH_4) and other VOCs in the presence of NO_x produces O_3. Thus, in such conditions, increasing NO_x by human activities should, in principle, lead to the increase in atmospheric oxidation capacity (OH and O_3) (Seinfeld and Pandis, 2006), and result in higher SOA yields. For example, using a chemical transport model, PMCAMx, Lane et al. (2008) suggested that a 50 % reduction in NO_x emissions could decrease predicted ground-level BSOA by an average of 0.5 μg m^{-3} in the eastern US by lessening the atmospheric oxidant levels.

Due to the multiple impacts of NO_x on SOA formation, it is important to understand how NO_x emission controls alter the particulate matter atmospheric loading. The goal of this study is to improve the SOA scheme in a global climate–chemistry model by incorporating a 4-product volatility basis set (VBS) framework (Pye et al., 2010), which has four representative volatility bins to better represent the volatility distribution of all semivolatiles in the atmosphere than the default 2-product scheme (Heald et al., 2008; Odum et al., 1996). The model is then used to investigate the impacts of anthropogenic NO_x emission reduction on SOA formation. Section 2 describes the observational data sets used in this study. In Sect. 3, we describe the default and updated SOA parameterizations embedded within the global chemistry–climate model framework. We perform control simulations using six different model configurations, including the default 2-product scheme and the updated SOA scheme with and without NO_x-dependent yields for monoterpene, and with and without simplified SOA aging parameterizations. Section 4 shows the results. The control simulations are evaluated and assessed against several observational data sets. Then, we perform sensitivity simulations to probe the impacts of a global 50 % anthropogenic NO emission reduction on SOA production. We conduct this experiment as a simplified potential future scenario based on the 50 % NO_x emission reduction from power plants in the southeast US by pollution control programs in the past decade (Frost et al., 2006; Kim et al., 2006). Section 5 summarizes the findings of this study.

2 Terminology and data sets

Table 1 summarizes major abbreviations used in this study. The term OA refers to the total particle-phase organic matter including carbon, hydrogen, oxygen and other possible elements. The term OC refers to only the mass of carbon in these organic compounds. Both OA and OC are used based on different measurement techniques. Similarly, primary organic carbon (POC) is the carbon mass in POA; secondary organic carbon (SOC) is the carbon mass in SOA. In this study the term SOA (secondary organic aerosol) and SOG (secondary organic gas) refer to particle phase and gas phase, respectively.

2.1 IMPROVE OC measurements

The US total OC data set is from the Interagency Monitoring of Protected Visual Environments (IMPROVE, Hand et al., 2011). IMPROVE OC is collected using quartz fiber filters for 24 h every third day, analyzed offline by thermal optical reflectance (TOR) (Chow et al., 1993), and corrected for an approximate positive artifact (Dillner et al., 2009). Assumptions made in this correction may not always be appropriate (Watson et al., 2009), and the potential negative artifacts due to the volatilization of particulate organics are not accounted for. We choose 120 surface sites from the IMPROVE network that are within the bottom layer in corresponding model grids. The original 3-day data from 2005 to 2009 have been averaged to seasonal and annual mean values. OC concentrations from sites within the same model grid cell ($1.9^\circ \times 2.5^\circ$ latitude by longitude) are averaged for comparison to modeled OC concentrations in corresponding model grid cells.

2.2 Aircraft-based OA measurements from an aerosol mass spectrometer (AMS)

The OA data sets come from 13 aircraft field campaigns that took place between 2005 and 2009 (Heald et al., 2011). In these campaigns, total OA density was measured using an AMS in standard temperature and pressure conditions (STP: 298 K, 1 atm) and provides fast online submicron aerosol composition (Canagaratna et al., 2007). For each field campaign, the 1 min raw data are averaged temporally and horizontally along the flight track for comparison to the simulated monthly mean OA vertical profile in the corresponding month and location in the model. Each observed OA profile is further averaged vertically to a single value for comparison to the simulated OA concentration averaged over the same range of altitudes.

2.3 Surface OA/OOA/HOA measurements from AMS

We select 42 surface AMS measurements in 2000–2008 from previous studies (Spracklen et al., 2011; Zhang et al., 2007) that differentiate between hydrocarbon-like OA (HOA, a surrogate for POA from combustion and biomass burning) and oxygenated OA (OOA, a surrogate for SOA from all sources). The HOA and OOA are determined by a multiple component analysis (MCA; Zhang et al., 2007). The averaged OOA, HOA and OA data for each campaign have been compared to the simulated monthly mean SOA, POA and total OA in the corresponding model grid. Most of these measurements were taken before 2005. We did not perform simulations in this period due to the lack of GEOS-5 meteorological data (described in Sect. 3.1). Therefore, the model results are averaged from 2005 to 2009 as a climatology to compare with this observational data set.

3 Modeling framework

3.1 CAM4-chem model

The global Community Atmosphere Model version 4 with chemistry (CAM4-chem) is part of the Community Earth System Model (CESM, version 1.2.2) (Tilmes et al., 2015). Here, we employ CAM4-chem in its specified dynamics mode, in which CAM and the Community Land Model (CLM) are driven by offline Goddard Earth Observing System model version 5 (GEOS-5) reanalysis meteorological fields (available since 2004). The prescribed sea surface temperature and sea ice data are from the Climatological/Slab-Ocean Data Model (DOCN) and Climatological Ice Model (DICE) as other components of CESM. In this configuration, CAM4-chem is run in a chemistry-transport model mode, such that direct comparison can be performed without having to consider variability associated with internally generated meteorology. CAM4-chem includes interactive simulation of O_3–NO_x–CO-VOC and bulk aerosol chemistry (based on the MOZART-4 chemical mechanism) as described in Lamarque et al. (2012). The default 2-product SOA scheme is described in Sect. 3.2 and in Heald et al. (2008). Updates performed for the purpose of this study are discussed in Sects. 3.3 and 3.4. The emissions of isoprene and monoterpenes are calculated online by the Model of Emissions of Gases and Aerosols from Nature (MEGAN 2.1), which is embedded in CLM (Guenther et al., 2012). The anthropogenic, biomass burning and other (except biogenic) emissions in CESM are as described in Lamarque et al. (2012). These consist of anthropogenic emissions from the Precursors of Ozone and their Effects in the Troposphere (POET) inventory for 2000 (Granier et al., 2005), with Asia replaced by the Regional Emission inventory for ASia (REAS v1) for each year (Ohara et al., 2007). The biomass burning emissions are from GFED-v2 (van der Werf et al., 2006) for 2005–2008 and from the Fire INventory of NCAR (FINN-v1) for 2009 (Wiedinmyer et al., 2011). All the SOA schemes discussed in this study consider that SOAs are only generated from oxidization of gas-phase VOCs. The SOA formation from organic compounds emitted originally in the condensed phase is not considered. Simulations are performed with a 30 min time

Table 1. Abbreviations used in this study.

Abbreviations	Description
OA	Organic aerosol, including the mass of carbon, oxygen and other possible elements (OA = POA + SOA).
OC	Organic carbon (OC = POC + SOC).
POA	Primary organic aerosol.
POC	Primary organic carbon.
SOA	Secondary organic aerosol.
SOC	Secondary organic carbon.
SOG	Secondary organic gas.
ASOA	Anthropogenic secondary organic aerosol.
BSOA	Biogenic secondary organic aerosol.
AVOC	Anthropogenic volatile organic compounds.
BVOC	Biogenic volatile organic compounds.
SOAM	SOA from monoterpene oxidation.
SOAI	SOA from isoprene oxidation.
MTP	Monoterpenes.
ISOP	Isoprene.
HOA	Hydrocarbon-like organic aerosol, a surrogate for POA.
OOA	Oxygenated organic aerosol, a surrogate for SOA.

step, a horizontal resolution of $1.9^\circ \times 2.5^\circ$ and 56 levels from the surface to approximately 40 km.

3.2 Default SOA parameterization

In CAM4-chem, the default SOA formation follows the 2-product approach (Odum et al., 1996). Each parent VOC is oxidized to generate 2 semivolatile surrogates, which can partition into pre-existing organic particles including both POA and SOA. The partitioning of the semivolatile products is described by absorptive partitioning theory into carbonaceous aerosol material (Donahue et al., 2006; Pankow, 1994). CAM-chem tracks POC in its emission, transport and deposition module. Later, in Sect. 4.2, we assume a POA-to-POC ratio of 1.4 (Aiken et al., 2008; White and Roberts, 1977) to calculate POA and OA to compare with observations. The model simulates anthropogenic SOA (ASOA) from NO_x-dependent OH-initiated oxidation of anthropogenic aromatics (benzene, toluene and xylene), BSOA from the OH-initiated oxidation of isoprene, and the ozonolysis, OH- and NO_3-initiated oxidation of monoterpene (Table 2). The surrogate SOA products are assumed to be $C_{10}H_{16}O_4$ for SOA from monoterpenes (SOAM), $C_5H_{12}O_4$ for SOA from isoprene (SOAI), and $C_6H_7O_3$, $C_7H_9O_3$, and $C_8H_{11}O_3$ for SOA from benzene, toluene and xylenes; therefore, the O : C ratio is constant for each SOA species. The overall O : C ratio in total OA depends on the split between POA and SOA, and the fraction of each SOA species. Fossil content is regarded as POA including both hydrophobic and hydrophilic compounds and is not included in SOA in CAM4-chem. The default 2-product model in CAM4-chem only applies low-NO_x yields parameterization for all OH- and O_3-initiated BSOA formation. The SOA mass yields (summarized in Table S1) are from Heald et al. (2008) and references therein.

3.3 Updated SOA scheme

We update the SOA model to include a 4-product VBS scheme, which has 4 semivolatile surrogates for each parent VOC species. The saturation concentrations (C^*) at 295 K for the 4 product groups are 0.1, 1, 10 and 100 $\mu g\,m^{-3}$, respectively. This VBS has a wider range of volatilities than the default 2-product parameterization that can better represent the volatility distribution of atmospheric semivolatiles. Another goal of implementing this VBS framework is to facilitate implementation of advanced processing including the aging effect. Changing the enthalpies of vaporization (see Tables S1 and S2 in the Supplement) has no significant effect on simulated SOA burden (difference smaller than 2 %). In addition to the current reactions used in the 2-product model, we have added the NO_x-dependent pathway for SOA formation from monoterpenes and the NO_3-initiated oxidation of isoprene into the VBS (see Table 2). SOA formed from OH-initiated photooxidation of isoprene still only has one set of yields following the low-NO_x parameterizations. We do not change this isoprene-SOA parameterization to remain consistent with the VBS framework from Pye et al. (2010). Additional simulations that include the high-NO_x pathway of isoprene chemistry are discussed in the Supplement. The SOA mass yields (summarized in Table S2) are from Pye et al. (2010) and references therein.

In the 4-product VBS model, the partitioning between the high-NO_x (RO_2+NO) and low-NO_x (RO_2+HO_2) pathway

Table 2. Summary of SOA treatments in CAM4-chem model runs.

SOA scheme	Reactions to form SOA	Description
2-product	MTP+OH(HO_2); MTP+O_3(HO_2); MTP+NO_3; ISOP+OH(HO_2); AVOCs+OH(HO_2); AVOCs+OH(NO).	Default 2-product scheme; SOA mass yields summarized in Table S1 (Heald et al., 2008).
VBS	MTP+OH(HO_2); MTP+O_3(HO_2); MTP+OH(NO); MTP+O_3(NO); MTP+NO_3; ISOP+OH(HO_2); ISOP+NO_3; AVOCs+OH(HO_2); AVOCs+OH(NO).	Updated 4-product VBS scheme; SOA mass yields summarized in Table S2 (Pye et al., 2010)
VBS_lowNO_x	MTP+OH(HO_2); MTP+O_3(HO_2); MTP+NO_3; ISOP+OH(HO_2); ISOP+NO_3; AVOCs+OH(HO_2); AVOCs+OH(NO).	Same as VBS, but assuming all monoterpene SOA (SOAM) is formed under low-NO_x conditions
VBS_agHigh	Same as VBS	Same as VBS, with multi-generational aging applied to all species; $k_{OH} = 4 \times 10^{-11}$ cm^3 molec^{-1} s^{-1}.
VBS_agLow	Same as VBS	Same as VBS, with multi-generational aging applied to all species; $k_{OH} = 5.2 \times 10^{-12}$ cm^3 molec^{-1} s^{-1}.
VBS_agAVOC	Same as VBS	Same as VBS, with multi-generational aging applied to ASOA only; $k_{OH} = 4 \times 10^{-11}$ cm^3 molec^{-1} s^{-1}.

is determined by the branching ratio β (Pye et al., 2010):

$$\beta = \frac{[NO]}{[NO] + [HO_2]}.$$

Thus, $100 \times \beta$ % of the parent hydrocarbon channels through the high-NO_x pathway, and $100 \times (1-\beta)$ % of the parent hydrocarbon channels through the low-NO_x pathway. This format of β is a simplification of

$$\beta = \frac{\sum k_{RO_2+NO} \times [NO]}{\sum k_{RO_2+NO} \times [NO] + \sum k_{RO_2+HO_2} \times [HO_2]},$$

where k_{RO_2+NO} and $k_{RO_2+HO_2}$ represent the reaction rate coefficients of RO_2+NO and RO_2+HO_2, respectively.

Field studies that quantified the elemental composition of OA indicate the importance of aged oxygenated OA (Aiken et al., 2008; Chen et al., 2011; Heald et al., 2010). Several regional modeling studies have found the "aging" process necessary to produce reasonable OA mass (Athanasopoulou et al., 2013; Hodzic and Jimenez, 2011; Knote et al., 2015; Lane et al., 2008; Tsimpidi et al., 2010). In this study we implement a simplified aging parameterization into the global model to provide a rough assessment of the SOA sensitivity in VBS to the effect of aerosol aging. At every model time step, each gas-phase SOA product except for the lowest volatility product ($C^* = 0.1\,\mu g\,m^{-3}$) is assumed to be further oxidized by OH with a reaction rate constant k_{OH} of 4×10^{-11} cm^3 molec^{-1} s^{-1} (Atkinson and Arey, 2003; Tsimpidi et al., 2010), which reduces its volatility by an order of magnitude. The oxygen-to-carbon ratio (O : C) is assumed to be constant for each surrogate SOA product; thus, an increase in SOA mass due to the addition of oxygen is not considered in the aging process. Considering the complexity of various SOA species and the large uncertainties in aging process, the assumption of a fixed O : C ratio for each SOA product surrogate is acceptable for global model parameterizations. The aging rate $k_{OH} = 4 \times 10^{-11}$ cm^3 molec^{-1} s^{-1} is at the high end of previously suggested parameters (Lane et al., 2008). We do simulations with and without this aging parameterization to quantify the possible range of global SOA strengths and additional simulations (see Sect. 3.4) to examine the effect of different aging parameters.

Particle-phase SOA as well as gas-phase SOG are removed from the atmosphere by wet and dry deposition. Dry deposition follows a resistance-in-series formulation (Heald et al., 2008; Wesely, 1998). SOA and other soluble aerosols are removed by both in-cloud scavenging and below-cloud washout (Barth et al., 2000; Lamarque et al., 2012).

3.4 Experiment setup

In this study, we apply six different treatments of SOA formation, as summarized in Table 2. 2-product is the default SOA model; VBS and VBS_agHigh are the updated 4-product VBS schemes with and without the aging effect. VBS_agHigh applies the high aging rate $k_{OH} = 4 \times 10^{-11}$ cm^3 molec^{-1} s^{-1} to all species, thus, presumably providing the higher bound of simulated SOA loadings. These three schemes (2-product, VBS and VBS_agHigh) are the

main SOA schemes that we use to compare with observations (Sect. 4.2) and study the sensitivity to NO_x perturbations. For each of the three schemes, we perform one control run and one sensitivity run in which anthropogenic NO emissions are reduced by 50 % (Sect. 4.3). We perform additional simulations to explore the impact of different aging and NO_x-dependency parameterizations: VBS_agLow applies a lower k_{OH} of 5.2×10^{-12} cm^3 molec^{-1} s^{-1} (Hu et al., 2013) to all species, which is close to the lower limit suggested by other studies (Hodzic and Jimenez, 2011; Spracklen et al., 2011); VBS_agAVOC applies $k_{OH} = 4 \times 10^{-11}$ cm^3 molec^{-1} s^{-1} to AVOCs only, as suggested by some studies that ASOA ages longer than BSOA (Lee-Taylor et al., 2015). VBS_lowNO_x is the same as VBS except that all SOAM is assumed to be formed through the low-NO_x (RO_2+HO_2) pathway. This VBS_lowNO_x scheme is done to isolate the influence of the NO_x-dependent pathway for SOAM formation, which is not considered in the default 2-product settings. All simulations are conducted for the years 2004–2009 with offline meteorology from GEOS-5 reanalysis and specific monthly anthropogenic emissions. The year 2004 result is discarded as spin-up.

4 Results

4.1 Comparison of various SOA schemes

The annual mean zonally averaged SOA concentration is shown in Fig. 1. The tropical maximum in the lower troposphere is due to large year-round Amazonian BVOC emissions coupled with extensive seasonal biomass burning that provides ample pre-existing POA onto which the semivolatiles can condense. The second surface maximum in the Northern Hemisphere mid-latitudes, 30–60°, is mostly attributed to (1) summertime BVOC emissions from broadleaf deciduous forest in the temperate and boreal zones, especially the southeast US which has very high BVOC emissions in the summer (Guenther et al., 2006); (2) plentiful supply of anthropogenic and biomass burning emitted POA; and (3) large amounts of AVOC emissions from human activities. In most simulations, indicated by the white contour lines in Fig. 1, the BSOA from isoprene and monoterpene oxidation accounts for more than 70 % of the total SOA in most latitudes and altitudes, which actually includes both "naturally formed" and "anthropogenically influenced" BSOA. The rest is ASOA from the oxidation of AVOCs. In the VBS_agAVOC run, ASOA accounts for a larger fraction in Northern Hemisphere mid-latitudes than other simulations ranging from 30 to 50 % because in this scheme the aging process is only applied to ASOA.

Table 3 details the annual global SOA budget in each control experiment. Compared to the default 2-product approach, the VBS scheme predicts a smaller global annual burden of SOA (19 % lower than the 2-product), although the surface concentration is 11 % higher with compensating lower concentrations at higher elevations. Due to the higher yields in the VBS (see Tables S1 and S2), more parent hydrocarbon is consumed near the source location and less is transported to the upper troposphere relative to the 2-product scheme. Their different volatility also contributes to the difference in SOA concentrations. Table 3 suggests a shorter SOA lifetime of 8.9 days in the VBS than the lifetime of 11.4 days in the 2-product scheme due to the larger wet-deposition flux, which is consistent with the higher surface concentration. The SOA global burden in the VBS_lowNO_x run is 14 % higher than the VBS. This is consistent with the fact that the high-NO_x (RO_2+NO) channel is less SOA-producing compared to the low-NO_x (RO_2+HO_2) channel. The yields of SOAM at 10 µg m^{-3} under high- and low-NO_x are 0.09 and 0.19, respectively (Table S2).

For present climate, the differences in annual burden between the two VBS models without aging effect (VBS and VBS_lowNO_x) and the 2-product model are relatively small (< 20 %), because for most parent hydrocarbon species they are fitted into the same chamber data (see Heald et al., 2008; Pye et al., 2010, and references therein). In contrast, in VBS_agHigh, adding the aging effect accelerates the shift of volatile mass towards lower volatility bins and hence more mass in the particle phase, and results in an overall doubling of the net SOA (particle phase) production, which is important for SOA environmental impacts. We find that the SOA production is sensitive to the assumed OH oxidation rate constant (k_{OH}) for aging of the semivolatile intermediates. For example, using VBS_agLow scheme with a lower k_{OH} of 5.2×10^{-12} cm^3 molec^{-1} s^{-1} (Hu et al., 2013), the annual mean SOA production rate would be 44.6 ± 2.0 Tg[C] year^{-1}, in comparison to a production rate of 58.6 ± 2.4 Tg[C] year^{-1} in the VBS_agHigh scheme with $k_{OH} = 4 \times 10^{-11}$ cm^3 molec^{-1} s^{-1}, and a production rate of 28.6 ± 1.6 Tg[C] year^{-1} in the VBS scheme without aging parameterization. This single aging parameter represents the multi-generational aging of hundreds of thousands of oxidation intermediate species that are involved in the SOA formation (Lee-Taylor et al., 2015) and is currently not well characterized for individual precursors and chemical environments. In the rest of this study, we will use the three schemes, 2-product, VBS and VBS_agHigh, to compare with observations and explore the NO_x-dependent effects.

4.2 Evaluation of OA in CAM4-chem simulations

4.2.1 Comparison with the IMPROVE network OC observations

The IMPROVE surface observations and the model outputs are averaged from 2005 to 2009. Modeled OC concentrations are calculated as the sum of primary carbon (directly emitted and transported in the model) and the carbon contained in each SOA species that is calculated assuming the surro-

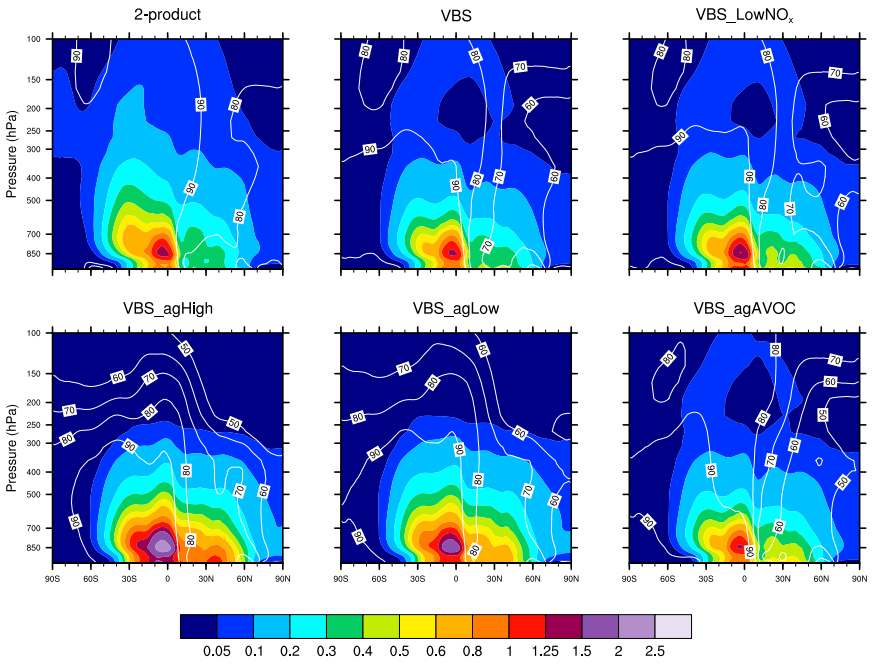

Figure 1. Annual mean zonally averaged SOA concentration (μg m^{-3}) (shown as colored shades) and the fraction of biogenic SOA (%) (shown as white contours) in CAM4-chem for different SOA treatments.

Table 3. Summary of simulated annual mean global budget of SOA (particle-phase).

	Burden Tg[C]	Net SOA production Tg[C] year^{-1}	Lifetime Day	Wet deposition Tg[C] year^{-1}	Other losses (by SOA dry deposition) Tg[C] year^{-1}
2-product	0.85 ± 0.04	27.3 ± 2.1	11.4 ± 0.4	-24.4 ± 1.8	-2.9 ± 0.3
VBS	0.69 ± 0.03	28.6 ± 1.6	8.9 ± 0.2	-25.3 ± 1.4	-3.3 ± 0.3
VBS_lowNO$_x$	0.79 ± 0.03	33.7 ± 1.8	8.5 ± 0.2	-29.8 ± 1.5	-3.9 ± 0.3
VBS_agHigh	1.08 ± 0.06	58.6 ± 2.4	6.7 ± 0.1	-52.1 ± 2.1	-6.5 ± 0.4
VBS_agLow	0.96 ± 0.05	44.6 ± 2.0	7.8 ± 0.1	-40.0 ± 1.7	-4.8 ± 0.3
VBS_agAVOC	0.75 ± 0.03	31.5 ± 1.6	8.6 ± 0.2	-27.8 ± 1.4	-3.7 ± 0.3

gate SOA products described in Sect. 3.2. Figures 2a and 3 show the model–IMPROVE comparison of annual mean surface total OC concentrations using the models 2-product, VBS and VBS_agHigh. The total OC in the 2-product and the VBS models are similar to each other and are close to the IMPROVE OC magnitude. They capture the observed spatial distribution to within 50 % ($r^2 = 0.45$ and 0.47, respectively). They capture the low OC values in the middle and west inland areas, and high OC values in the southeast US where considerable BVOC is emitted from forest as well as POC and AVOC emitted from economic sectors. In the northeast US and some coastal polluted regions in California, OC is greatly overestimated by the models. Figure 2c indicates large simulated POC concentrations in these regions while IMPROVE total OC ($=$ POC $+$ SOC) is not even as large as the simulated POC concentrations. Therefore, the positive bias of the two no-aging simulations in the northeast US is likely due to an overestimate of POC emissions in the inventory or due to the assumption that all POAs are non-volatile once emitted and stay in the particle phase until deposition. The fact that IMPROVE sites are predominantly located in remote clean regions might also contribute to this discrepancy. In Fig. 2b the white contour lines illustrate the annual mean fraction of SOC in total OC. Table 4 summarizes the fractions in each season. In the two no-aging models, the annual mean SOC-to-OC ratio ranges from 20 to 30 % in the northeast US and from 40 to 60 % in the southeast US. Even in summer, the ratio does not exceed 50 % in the northeast US and 70 % in the southeast US, which is lower than the suggested values from Ahmadov et al. (2012) and Shrivastava et al. (2008). The aging experiment VBS_agHigh increases the SOC-to-OC ratio greatly (68 and 81 % in summertime northeast and southeast US) and overestimates OC across the entire US due to large SOA formation from aging, which is consistent with previous studies in that the aging coefficient we apply here ($k_{OH} = 4 \times 10^{-11}$ cm^3 molec^{-1} s^{-1}) is at the

Table 4. Fraction of SOC in total OC (%) in the southeast US and the northeast US.

		Annual	MAM	JJA	SON	DJF
Northeast US	2-product	24 %	15 %	45 %	20 %	6 %
	VBS	28 %	19 %	49 %	23 %	8 %
	VBS_agHigh	45 %	33 %	68 %	39 %	12 %
Southeast US	2-product	39 %	29 %	62 %	32 %	8 %
	VBS	44 %	34 %	67 %	37 %	10 %
	VBS_agHigh	63 %	55 %	81 %	56 %	18 %

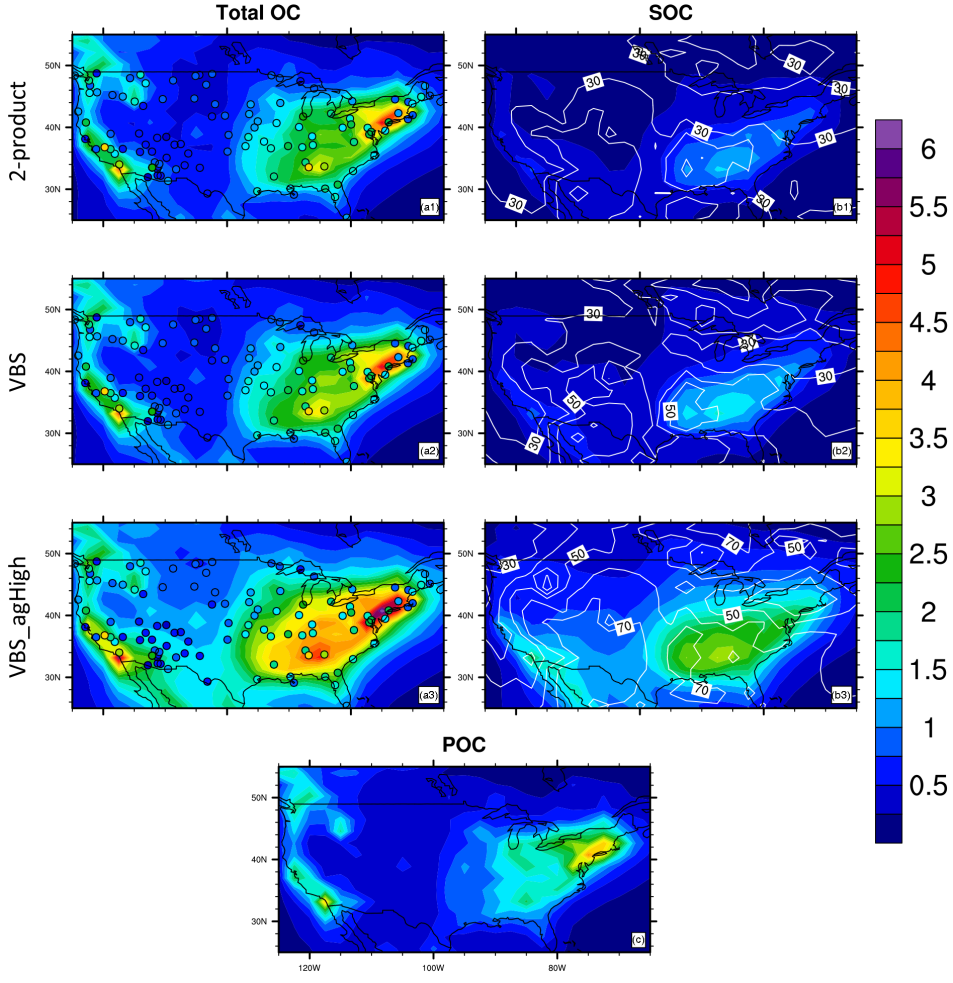

Figure 2. Annual mean surface concentrations (units: μg[C] m^{-3}) of **(a1)–(a3)** total organic carbon (OC = POC + SOC), **(b1–b3)** secondary organic carbon (SOC) and **(c)** primary organic carbon (POC). The data is averaged from 2005 to 2009. In **(a1)–(a3)**, scatters are IMPROVE observations and color shades are simulated total OC from the models 2-product, VBS and VBS_agHigh. In **(b1)–(b3)**, white contours indicate the fraction of SOC in total OC (%), ranging from 30 to 70 % with an interval of 10 %. **(c)** shows simulated POC, which is identical in the three simulations.

high end of suggested aging rates. The VBS_agHigh scheme slightly improves the replication of spatial distribution of annual mean OC concentrations ($r^2 = 0.53$ as compared to 0.45 and 0.47 in the 2-product and VBS schemes) but not in summer ($r^2 = 0.13$, Table 5). Assuming only ASOA ages, the VBS_agAVOC scheme does not improve the simulated spatial distribution ($r^2 = 0.48$ in annual average and $r^2 = 0.18$ in summer; Table 5).

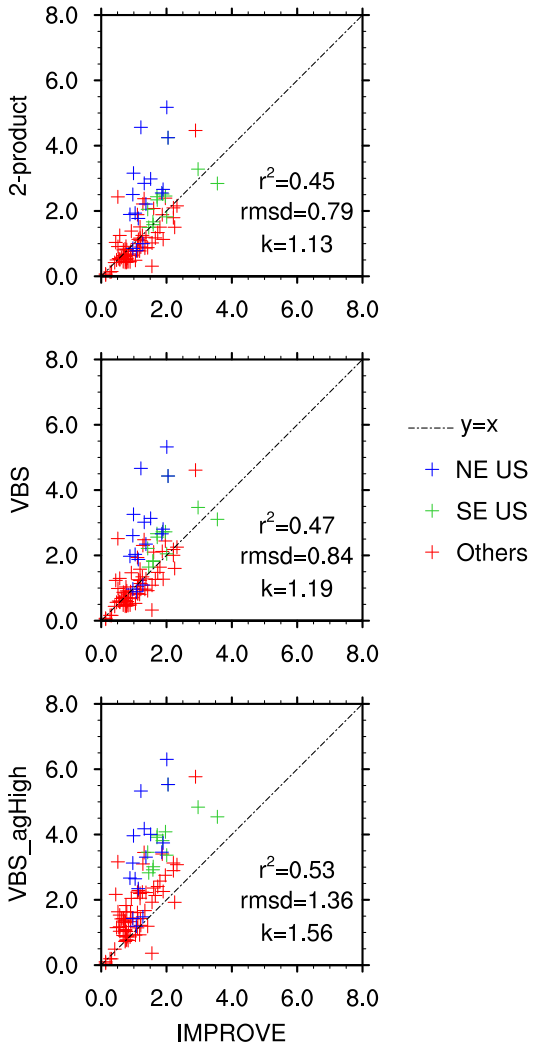

Figure 3. Comparison of averaged annual mean surface OC concentrations (μg[C] m^{-3}) between IMPROVE measurements and the three simulations: 2-product, VBS and VBS_agHigh. Different colors indicate sites in different regions. In each subplot, the dashed line is the 1 : 1 line. The coefficients of determination (r^2), root-mean-square difference (rmsd) and the model-to-observation slope (k) are included.

Table 5. Coefficients of determination (r^2) of IMPROVE measurements versus simulated total OC.

	Annual	MAM	JJA	SON	DJF
2-product	0.45	0.40	0.18	0.41	0.42
VBS	0.47	0.42	0.18	0.43	0.42
VBS_agHigh	0.53	0.54	0.13	0.49	0.45
VBS_agAVOC	0.48	0.45	0.18	0.44	0.44

4.2.2 Vertical profiles of OA from aircraft-based AMS measurements

To assess the simulated OA vertical profile in these models, we select 13 aircraft campaigns that had available AMS measurements between 2005 and 2009. The comparison of vertical profiles is shown in Fig. 4. The VBS_agHigh scheme provides a higher OA concentration than the other two no-aging simulations. Overall, the intermodel differences are smaller than the model–observation differences. In biomass-burning-influenced regions, the observed OA profile is usually associated with large variations at elevated altitude, indicating sporadic fire plumes. For example, for the AMMA campaign (west Africa), the aircraft tracked biomass-burning plumes, thus giving several maxima of observed mean OA at multiple altitudes. In this case, the observed median value at each layer is a more reliable value for evaluation of the simulations (Heald et al., 2011). The simulated OA profiles in these fire-influenced regions are close to the observed median OA profiles and all are within 1 standard deviation of observations except at site DODO (west Africa). The enhanced observed concentrations in DODO in the upper troposphere indicate strong deep convection. The discrepancies are likely caused by biases in subgrid meteorology and vertical transport rather than the chemical formation of SOA or POA emissions. Polluted regions have high OA concentrations at the surface. All three of the simulations capture both the vertical distribution characteristics and magnitude of concentration with the largest model–observation difference within 5 μg m^{-3}. OA in remote sites is close to zero. The models capture OA at IMPEX (west North America and east Pacific) and OP3 (Borneo) sites but overestimate at TROMPEX (Cabo Verde) and VOCALS-UK (South Pacific). Generally, the simulated OA profiles are all within a factor of 2 of the observed magnitude, indicating a reasonable model performance across different regions and seasons. Figure 5 compares OA concentrations averaged across each entire campaign. All three simulations underestimate observed OA in most campaigns, except in the remote sites of TROMPEX (Cabo Verde) and VOCALS-UK (eastern South Pacific). The VBS_agHigh scheme has the lowest root-mean-square difference (rmsd) of 1.45 and captures 56 % of observed OA mean concentrations, as compared to 50 and 52 % in the 2-product and VBS schemes.

4.2.3 OA, SOA and POA from surface AMS measurements

The observed OOA is a surrogate for SOA, and HOA is a surrogate for POA in AMS measurements (Aiken et al., 2009; Lanz et al., 2007; Zhang et al., 2005). We use 42 short-term surface AMS measurements (Spracklen et al., 2011; Zhang et al., 2007) and classify their locations into four groups: North America (17 sites), Europe (12 sites), East Asia (12 sites) and Amazon (1 site). Most of these measurements were taken before 2005. The 2005–2009 monthly

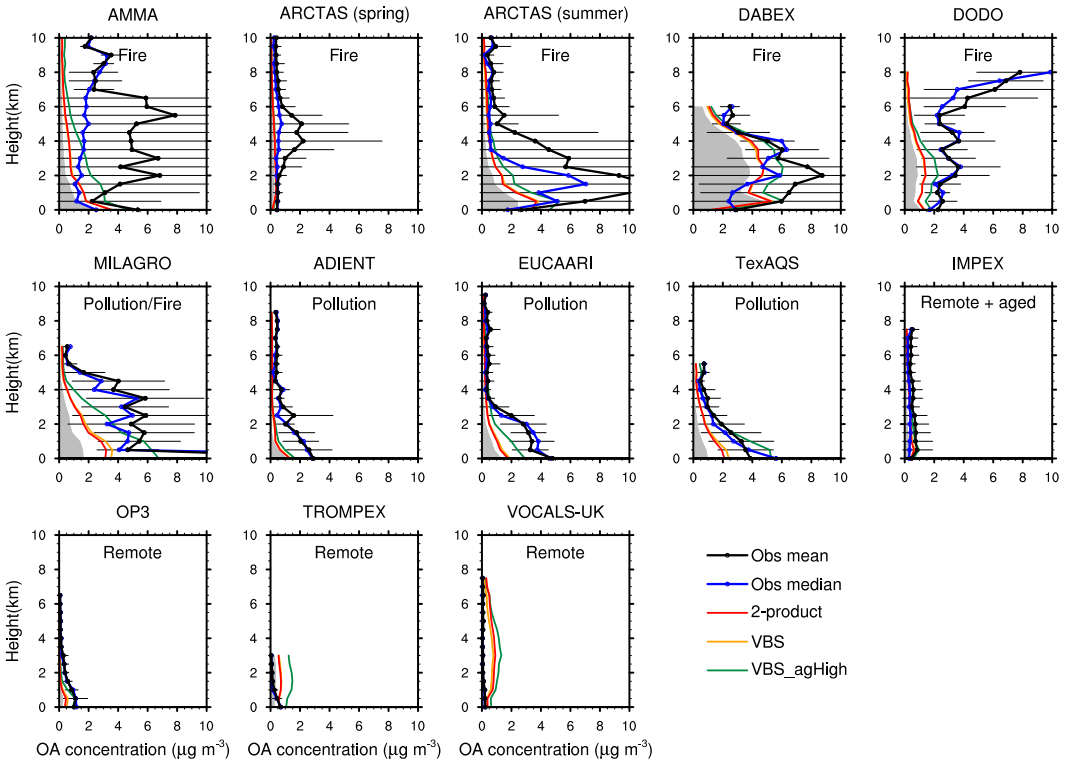

Figure 4. Comparison between the observed vertical profiles of OA concentration ($\mu g\,m^{-3}$) from 13 AMS field campaigns and the three model simulations: 2-product, VBS and VBS_agHigh. The campaign information is summarized in Heald et al. (2011) (Fig. 1 and Table 1 therein). The error bars are 1 standard deviation of the binned observations for each 0.5 km interval. The grey shades are simulated POA assuming a POA-to-POC ratio of 1.4. The model simulations are sampled for the corresponding months and locations for each campaign. The location and location type for each campaign is included in each subplot.

mean model results have been averaged into a climatology to compare to the observations, which may lead to large model–observation differences. Figure 6 compares the measured and simulated OA, OOA(SOA) and HOA(POA). The comparisons between observations and simulations show large discrepancies (in opposite directions) for primary and secondary species. POA is identical in the three simulations. Consistent with the comparison to the IMPROVE network in Sect. 4.2.1, the models overestimate POA in most regions and especially in North America, which will promote condensation of semivolatiles onto pre-existing organic matter, thus forming more SOA. The SOA concentrations in the two no-aging models, 2-product and VBS, are close to observed OOA in North America and lower in other regions. By including the aging, the VBS_agHigh simulation increases SOA concentration, leading to an overestimation in North America and still an underestimation in most other regions. The total OA concentrations in all models exceed observed OA in North America. In Fig. 7 we plot the comparison of SOA(OOA)-to-OA ratios from the observations and simulations. The 2-product and VBS models significantly underestimate the observed OOA-to-OA ratios that range from 0.4 to 1. The VBS_agHigh model makes an improvement but is still lower than the observations due to the large amount of simulated POA. Overall, the intermodel differences are smaller than the model–observation differences. These conclusions are consistent with Sect. 4.2.1 and 4.2.2.

4.3 The impact of anthropogenic NO_x pollution on surface SOA

For each of the 2-product, VBS and VBS_agHigh schemes, we perform a control run and a sensitivity run in which the anthropogenic NO emissions are reduced by 50 % to explore the impact of NO_x pollution on surface SOA concentrations. Other NO sources including biomass burning and soil emissions are not changed. The 50 % reduction in anthropogenic NO emissions leads to a 36 % decrease in annual mean total NO emissions and a 38 % decrease in surface NO_x concentrations at global scale (Fig. S1 in the Supplement). The global surface level of oxidants OH, O_3 and NO_3 decrease by 13, 8 and 29 %, respectively (Fig. S2). The surface $NO:HO_2$ ratio has been greatly reduced by 67 %, while the change in branching ratio ($\beta = \frac{NO}{NO+HO_2}$) is small ($-3.4$ %), indicating the NO concentration in the model is too high for HO_2 to compete. The spatial distribution and probability density function of β are plotted in Figs. S3 and

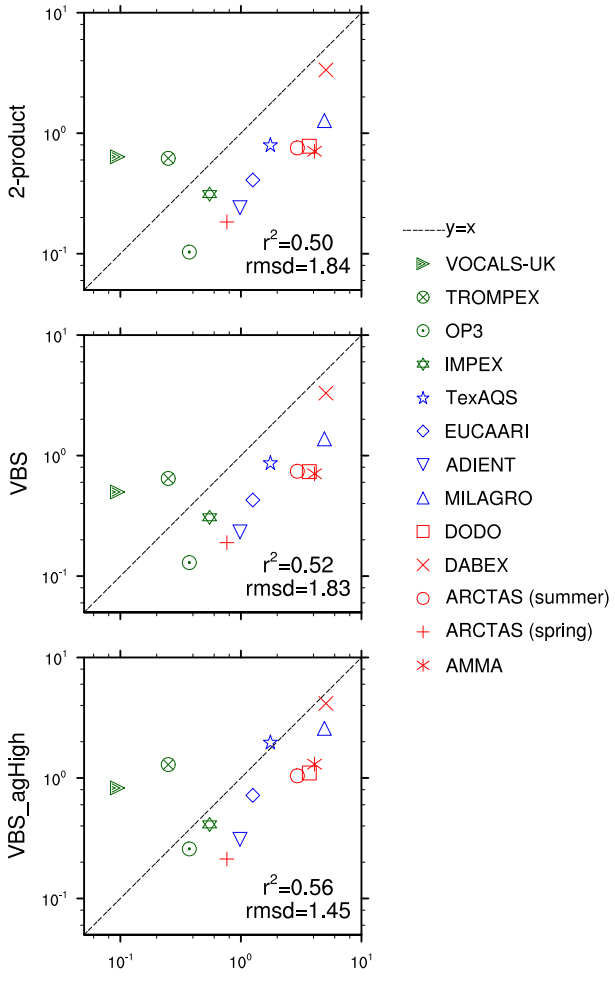

Figure 5. Comparison between averaged OA concentration ($\mu g\,m^{-3}$) from 13 AMS field campaigns and the three model simulations: 2-product, VBS and VBS_agHigh. The campaign information is summarized in Heald et al. (2011) (Fig. 1 and Table 1 therein). All data in each campaign are temporally, horizontally and vertically averaged to a single value and compared to the model outputs averaged over the same period and location.

S4 in the Supplement. We choose a polluted and a clean region as examples: the southeast US (32–40° N, 95–77° W) and the Amazon (17° S–5° N, 77–55° W), both of which are mostly in the NO_x-limited regime in terms of ozone formation due to their large BVOC emissions (Lane et al., 2008), i.e., the concentration of O_3 and OH are positively related to concentration of NO_x. We examine the dependence of annual mean surface SOA concentrations on β and oxidants level at the global scale and over the southeast US and Amazon regions in Fig. 8. The comparison of the sensitivity (red) and the control runs (green) indicates that the 50 % reduction in anthropogenic NO emissions leads to a small decrease in β, oxidation level and SOA concentrations. In Fig. 8, the small SOA concentrations associated with small β values ($\beta < 0.6$) mostly happen over the ocean (not shown) or polar regions where VOC precursors hardly exist and NO_x concentrations are low. In the range $0.6 < \beta < 1.0$, the common regime over land, the highest SOA concentrations occur at relatively lower β values, which are mostly located in tropical rain forests with large BVOC emissions and high SOA production efficiency through the low-NO_x pathway. The influences of β and oxidant level are tightly related because high β indicating high NO_x is usually associated with high concentrations of oxidants. The dependence of SOA on oxidant concentration indicates a maximum at medium oxidant level of approximately 0.8×10^{12} molec cm^{-3}. The low SOA concentrations at high oxidant level mostly occur in polluted regions where SOA production is overwhelmingly dominated by the high-NO_x (low-yields) pathway.

The SOA production in response to NO_x perturbations is complex, as described in Sect. 1. For example, in the VBS_agHigh scheme, we consider monoterpene SOA (SOAM) coming from NO_3-initiated oxidation and the low- and high-NO_x pathway for both OH- and O_3-initiated oxidation. As shown in Fig. 9, with a 50 % reduction in anthropogenic NO emissions, total surface SOAM concentration decreases, dominated by the decrease in NO_3-oxidation branch. This decrease in total SOAM mass is a result of addition or cancellation of various changes in each branch, and the relative importance of different branches may change with different regions. One interesting phenomenon is that when NO_x emissions are reduced, the low-NO_x OH- and O_3-initiated oxidation branches form less SOAM mass in the Amazon but more SOAM in human-influenced regions like mid-latitude broadleaf forest in the southeast US, coastal Asia and boreal forest in northern Europe. To further understand and quantitatively evaluate the complex NO_x influence on SOA formation, we examine the predicted change in surface SOA concentrations in different pathways in response to the decrease in anthropogenic NO emissions, as illustrated by Fig. 10. Table 6 details the relative contribution of each pathway to the total SOA change. The results for various SOA types, i.e., aromatic SOA, isoprene SOA and monoterpene SOA, are discussed below.

4.3.1 Anthropogenic SOAs from benzene, toluene and xylenes (ASOA)

ASOA in the three models are assumed to form from OH-initiated oxidation, including both low-NO_x and high-NO_x pathways, i.e., AVOCs+OH(HO_2) and AVOCs+OH(NO). In the southeast US as shown in Fig. 10, all models predict an increase in the low-NO_x pathway and a decrease in the high-NO_x pathway. This is because the model assumes linear interpolation between low- and high-NO_x pathways based on the branching ratio (Sect. 3.3). When NO_x is reduced, more AVOCs are oxidized under the low-NO_x pathway, which has higher yields (see Tables S1 and S2). Due to the limited change in β, the effect of shifting to a high-yield HO_2 pathway is very small. The total ASOA formation

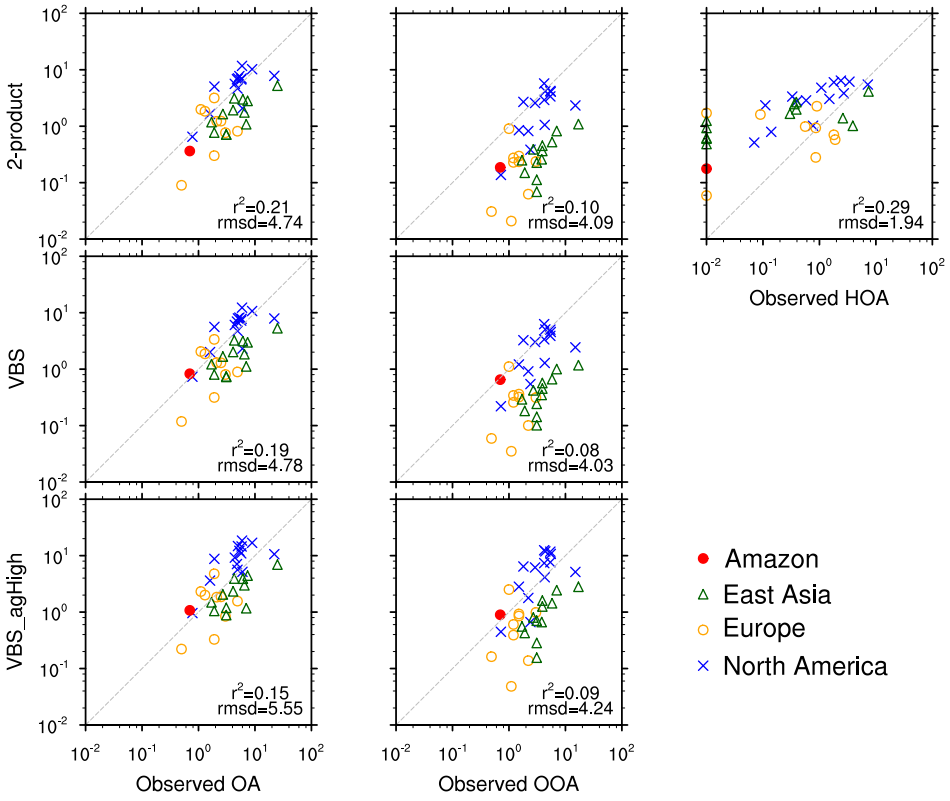

Figure 6. Comparison of surface AMS measurements (units: $\mu g\,m^{-3}$) and three simulations. First column: total OA; second column: SOA(OOA); third column: POA(HOA). The r^2 and rmsd are included in each subplot. The OOA is a surrogate for SOA from all sources. The observed HOA is a surrogate for POA from combustion and biomass burning. Simulated POA is identical in the three simulations. In the POA-HOA comparison, data points with observed HOA smaller than 0.01 $\mu g\,m^{-3}$ have been set to 0.01 $\mu g\,m^{-3}$ to be shown in the plots.

Table 6. The relative contributions (%) of each SOA formation pathway to the total SOA concentration change in the southeast US and the Amazon, defined as $\frac{\text{SOA change in each pathway}}{|\text{total SOA change}|}$. The sums of all numbers in each simulation equal −100 % because the total SOA change in the sensitivity runs compared to the control runs are always negative. The reaction denotations are the same as defined in Fig. 10.

		M1	M2	M3	M4	M5	I1	I2	A1	A2
SE US	2-product	−10.4		+15.0		−65.3	−46.8		+10.6	−3.1
	VBS	+2.9	−13.5	+29.5	+8.8	−63.8	−40.3	−32.7	+13.7	−4.5
	VBS_agHigh	+1.0	−5.3	+8.9	+2.0	−48.9	−35.1	−18.9	+3.5	−7.2
Amazon	2-product	−5.1		−0.2		−65.0	−30.8		+1.4	−0.4
	VBS	+0.4	−7.8	+5.9	−15.8	−45.1	−16.2	−21.9	+0.9	−0.5
	VBS_agHigh	−1.4	−4.3	−9.5	−13.9	−27.2	−30.4	−12.6	0.0	−0.6

depends on both the low-/high-pathway partitioning and the oxidation capacity, so it can either increase (e.g., 2-product, VBS) or decrease (VBS_agHigh). In the Amazon, the ASOA changes follow the same pattern as in the southeast US, but their relative contributions are very small due to the low concentrations of AVOCs and anthropogenic NO_x. The contributions of ASOA changes to the total SOA change (defined as $\frac{\text{change in ASOA}}{|\text{total SOA change}|}$) range from −3.7 to 9.2 % in the southeast US and from −0.6 to 1.0 % in the Amazon.

4.3.2 Isoprene SOA (SOAI)

In our current models, the isoprene only has one set of yields for OH-initiated daytime oxidation following low-NO_x parameterization and is oxidized by NO_3 during the night (the latter is not considered in the 2-product model). The OH oxidation is the dominant branch to form SOAI in both regions. When anthropogenic NO emissions are halved, both OH- and NO_3-initiated branches decrease in the southeast US and the Amazon due to reduced atmospheric OH and

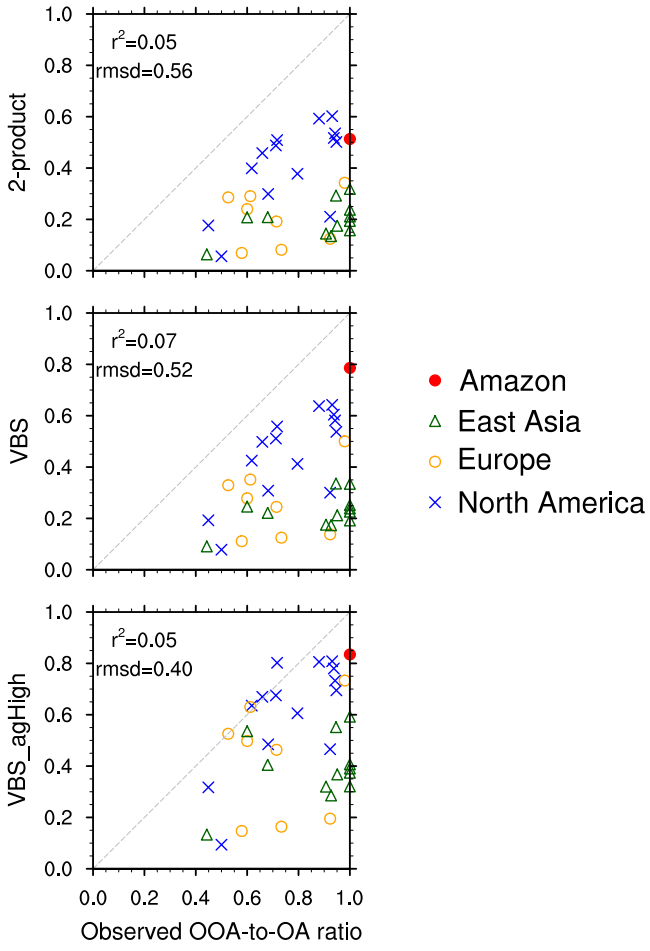

Figure 7. Comparison of observed OOA-to-OA ratio from surface AMS measurements and simulated SOA- to-OA ratio from the 2-product, VBS and VBS_agHigh schemes. r^2 and rmsd are included in each subplot.

NO_3 levels, respectively. The contributions of SOAI changes ($\frac{\text{change in SOAI}}{|\text{total SOA change}|}$) are −46.8 to −73.0 and −30.8 to −43.0 % in the two regions.

4.3.3 Monoterpene SOA (SOAM)

Monoterpenes are oxidized by OH, O_3 and NO_3 in all models but the 2-product model only considers the low-NO_x pathway (Table 2). In the southeast US with large human influence, the surface SOAM formation is largely attributed to NO_3-initiated oxidation as indicated by most models, which dominates the reduction in response to reduced NO_x. This branch itself contributes to the total SOA change ($\frac{\text{change in SOAM from NO}_3\text{−oxidation}}{|\text{total SOA change}|}$) by −48.9 to −65.3 %. This reduction in NO_3 branch compared to its normal value is relatively small because the decrease in NO_3 concentration is only 24 %. In the VBS and VBS_agHigh models, the partitioning between high- vs. low-NO_x pathways determines the tendency of increasing yields from the low-NO_x pathway and decreasing yields through the high-NO_x pathway. The OH oxidation in the southeast US follows such tendency. However, the SOA formed from both high- and low-NO_x pathways of ozonolysis increases. One possible explanation is the "buffering" between O_3- and NO_3-initiated oxidation, both of which mostly happen at night. Compared to the control run, NO_3 is significantly lower in the sensitivity run; thus, more monoterpenes would be oxidized by O_3 under both low- and high- NO_x conditions. Adding up the changes in all branches, the SOAM change contributions to total SOA change are about −36.1 to −60.7 %. In the Amazon's pristine environment, most branches demonstrate a slight reduction in SOAM in all models. Since the absolute magnitude of anthropogenic NO_x is small, the major influence of the NO_x might be the decline in level of atmospheric oxidants: OH, O_3 and NO_3 decrease by 14, 6 and 16 %, respectively. Despite the minor lessening of oxidation capacity, the SOAM reduction and total SOA reduction are negligible.

4.3.4 Summary of surface SOA concentration change

The changes in total SOA concentration at the surface in different regions are summarized in Table 7. In both human-influenced and clean regions, the 50 % reduction in anthropogenic NO emissions leads to a decline of BSOA, which dominates the overall SOA decrease. The ASOA could either increase (in models without aging parameterization) or decrease (in models with aging considered). Among the multiple effects of NO_x, BSOA is mostly influenced by changes in NO_3-initiated oxidation. Both BSOA and ASOA are also influenced by the change in atmospheric oxidation capacity and the partitioning between high- vs. low-NO_x pathways.

The annual mean total surface SOA reductions in the southeast US, the Amazon and global average range from 119 to 518, 30 to 153, 3.6 to 43 ng m^{-3}, respectively. The corresponding percentage reductions are 6.4–12.0, 0.9–2.8 and 0.9–5.6 %. These changes are comparable with previous estimates (Carlton et al., 2010;Lane et al., 2008) but all are smaller than the magnitude of 1 standard deviation, indicating that such changes are not statistically significant compared to interannual variations caused by climate and emission variations. The column concentrations of tropospheric SOA are also examined (results not shown here), and the conclusion still holds – no significant change of SOA column concentration when anthropogenic NO emissions are reduced by 50 %. One major reason is the small reduction in branching ratio β, which limits the shift between high- vs. low-NO_x chemical regimes. The fact that SOA is stable in response to anthropogenic NO_x changes is also attributed to the buffering of various branches (e.g., increased ozonolysis and decreased NO_3 oxidation), the partitioning between low- and high-NO_x pathways and the offset from opposite tendencies of BSOA and ASOA responses (in the no-aging models).

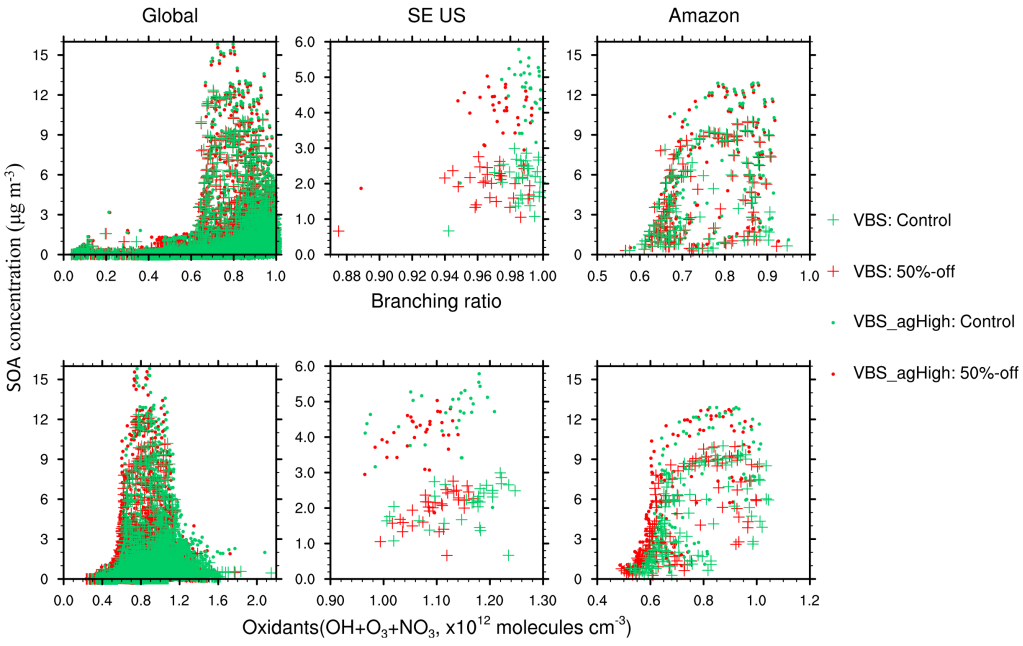

Figure 8. Dependence of annual mean surface SOA concentration ($\mu g\,m^{-3}$) on branching ratio and oxidants level at global scale, in the southeast US and the Amazon. The control runs and the sensitivity runs using VBS and VBS_agHigh schemes are shown. The 2-product results are similar to the VBS results (not shown). Data points over ocean are excluded. Note that the scales for the southeast US are different from the Amazon and the global subplots.

Table 7. Changes in surface SOA concentrations due to a 50 % reduction in anthropogenic NO emissions. Total SOA changes from each model are listed for global average, the southeast US and the Amazon.

		Concentration in control run ($ng\,m^{-3}$)	Standard deviation ($ng\,m^{-3}$)	Concentration change in sensitivity run ($ng\,m^{-3}$)	Percentage change
SE US (32–40° N, 95–77° W)	2-product	1638	248	−119	−7.3 %
	VBS	2005	286	−127	−6.4 %
	VBS_agHigh	4331	594	−518	−12.0 %
Amazon (17° S–5° N, 77–55° W)	2-product	3360	1383	−30	−0.9 %
	VBS	3884	1197	−46	−1.2 %
	VBS_agHigh	5390	1542	−153	−2.8 %
Global average	2-product	358	40	−3.6	−1.0 %
	VBS	393	37	−3.6	−0.9 %
	VBS_agHigh	774	52	−43	−5.6 %

5 Summary

NO_x plays a complex role in the chemical formation of SOA. The complexity includes the competition between NO and HO_2 to react with RO_2, its substantial influence on atmospheric oxidation capacity, and the nighttime NO_3 direct oxidation of isoprene and monoterpenes. In this study, we have updated the SOA scheme in the global chemistry–climate model CAM4-chem to include a 4-product VBS scheme that has a broader representation of volatility distribution and quantitatively evaluated and explained the multiple impacts of anthropogenic NO_x on SOA at global scale.

We updated the SOA scheme in CAM4-chem to a 4-product VBS scheme. Compared to the default 2-product model, the VBS scheme has 11 % higher surface SOA concentration. While the total annual mean SOA burden is 19 % smaller (0.69 ± 0.03 Tg[C] as compared to 0.85 ± 0.04 Tg[C]) and has a lifetime that is shorter (8.9 ± 0.2 days as compared to 11.4 ± 0.4 days). Due to the different volatility and higher yields of SOA in the VBS, more VOC is oxidized near the surface and less is transported to higher levels, and more SOA is washed out near the surface. We explored an aging parameterization with a constant reaction rate with OH ($k_{OH} = 4 \times 10^{-11}\,cm^3\,molec^{-1}\,s^{-1}$, the higher-limit in previous

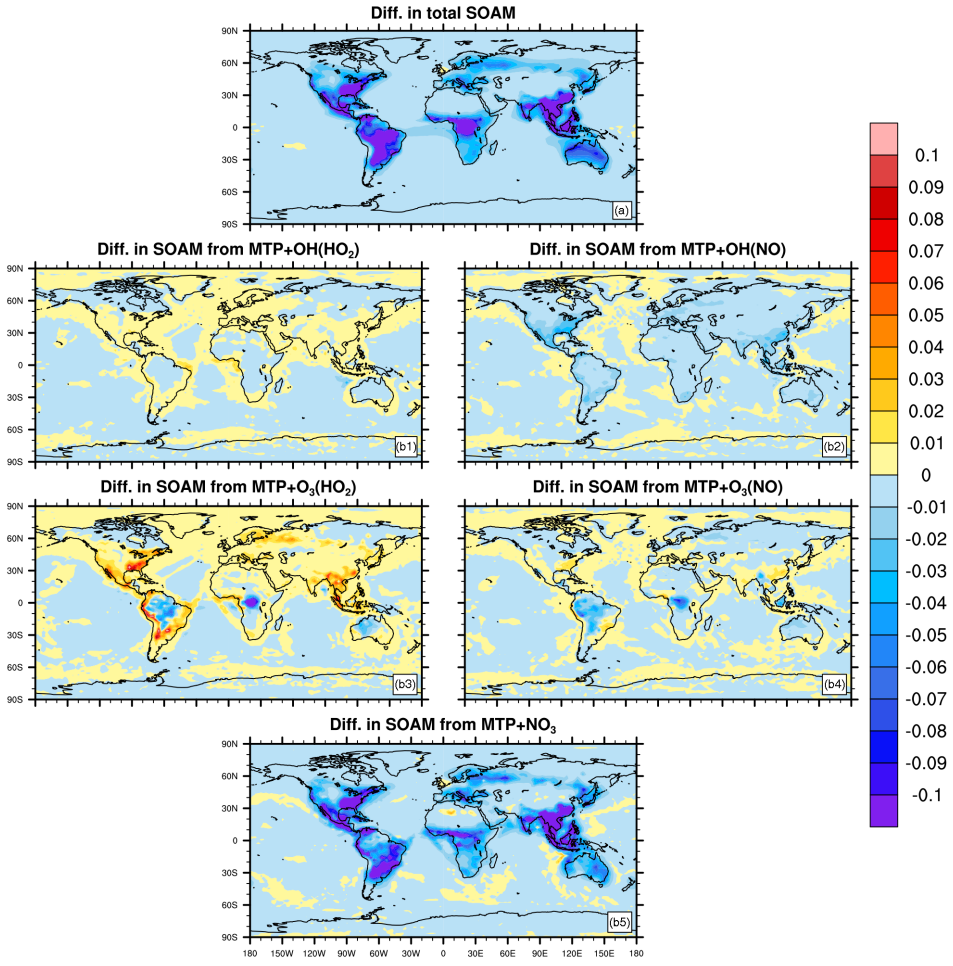

Figure 9. Changes in SOAM concentration ($\mu g\,m^{-3}$) in the sensitivity run with 50 % reductions in anthropogenic NO emissions compared to the control run using the VBS_agHigh scheme. The total SOAM change is shown in **(a)**. The SOAM change in each formation branch is denoted as **(b1)** MTP+OH(HO_2) (low-NO_x OH-photooxidation), **(b2)** MTP+OH(NO) (high-NO_x OH-photooxidation), **(b3)** MTP+O_3(HO_2) (low-NO_x ozonolysis), **(b4)** MTP+O_3(NO) (high-NO_x ozonolysis), and **(b4)** MTP+NO_3 (NO_3-initiated oxidation).

studies), which almost doubles the net annual SOA production and significantly increases the SOA concentration both at the surface and in the lower free troposphere. The global SOA burden with aging considered (i.e., VBS_agHigh scheme) increases to 1.08 ± 0.06 Tg[C] and the corresponding lifetime is 6.7 ± 0.1 days. By applying a lower aging reaction rate ($k_{OH} = 5.2 \times 10^{-12}\,cm^3\,molec^{-1}\,s^{-1}$, the lower-limit in previous studies), we found that the simulation of SOA is quite sensitive to the assumed k_{OH}. Despite the significance to SOA formation and properties, the aging effect is still poorly understood at the global scale. Further laboratory and process-modeling constraints at different conditions are needed.

The simulated total OC concentrations in the 2-product and the VBS models without aging are similar, and they capture the magnitude and distribution of annual mean surface OC concentrations in the US from the IMPROVE network, by 45–47 %, but overestimate OC in the polluted northeast US and western coastal regions. The model with an implementation of aging (VBS_agHigh) slightly improves the replication of annual mean spatial distribution ($r^2 = 53\,\%$) but overestimates the magnitude. All three models perform poorly in summertime. Compared to AMS measurements from 13 aircraft-based field campaigns, the simulations of OA vertical profiles are within a factor of 2 across different regions and seasons. The VBS_agHigh scheme performs better than the two no-aging models to reproduce these observed OA concentrations ($r^2 = 56\,\%$, rmsd = 1.45). Further climatological comparisons with surface AMS observations indicate reasonable simulated total OA concentrations but overestimation of POA in some polluted regions, which is consistent with the comparison to the IMPROVE network. This overestimation of POA may come from a higher biased POC from the emissions inventory in certain regions (e.g., the northeast US). If so, it would partially conceal the fact that the current parameterized SOA yields and overlooking of ag-

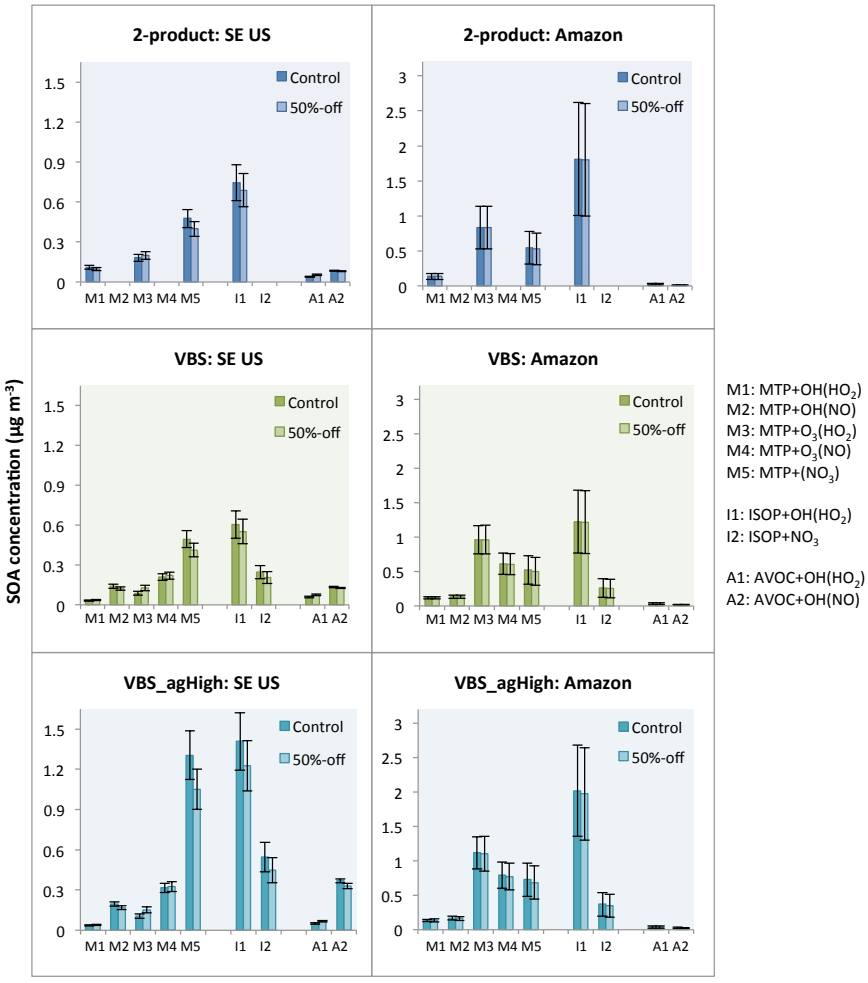

Figure 10. Annual mean surface SOA concentration ($\mu g\,m^{-3}$) in the control runs and the sensitivity runs (with 50 % anthropogenic NO emission off) from different pathways, averaged over the southeast US (32–40° N, 95–77° W) and the Amazon (17° S–5° N, 77–55° W).

ing in the two no-aging models actually lead to the SOA underestimation. Another possible explanation might be POA re-evaporation and subsequent conversion to SOA (Robinson et al., 2007), indicated by the lower fraction of the SOA-to-OA ratio in simulations than in the AMS observations. Generally, the intermodel differences are smaller than the model–observation differences. We believe that the updated SOA model (e.g., VBS, VBS_agHigh) is superior to the default one because we implemented the NO_x-dependent SOA formation of monoterpenes, whose absence is a major drawback of the default model. The VBS framework also facilitates inclusion of important processes like aging and the future implementation of size-resolved calculations. The model–observation discrepancies have several reasons: (1) potential loss of POA due to evaporation and subsequent SOA formation, which is currently not considered in this study; (2) uncertainties in chamber-derived SOA yields due to wall losses (Zhang et al., 2014); and (3) lack of constraints on dry deposition of organic gases (Hodzic et al., 2015; Knote et al., 2015) or unaccounted photolysis reactions during aging of organics (Hodzic et al., 2015). Other non-chemistry reasons include (1) the site-level measurement versus coarse model grid (1.9° × 2.5°), (2) specific observation time period (days to weeks) versus simulated monthly mean values, (3) subgrid meteorology (e.g., convection events) that the model cannot capture, and (4) large uncertainties related to fire activity (e.g., biomass burning plumes).

Finally, we performed sensitivity experiments to examine how the SOA loading responds to a 50 % reduction in anthropogenic NO emissions in different regions. The BSOA generally decreases due to the reduction in NO_3-initiated reaction and the reduced atmospheric oxidation capacity, while the ASOA increases in the two no-aging models mainly because of the increased partitioning to the low NO_x pathway; more AVOCs are oxidized through the low-NO_x pathway that has higher yields. In the aging model, ASOA decreases due to the more important effect of reduced oxidation capacity. Decreases in the total surface SOA concentra-

tions are 6.4–12.0, 0.9–2.8 and 0.9–5.6 % for the southeast US, the Amazon and global NO_x perturbations, respectively, which, however, are not significant. The fact that SOA formation is stable to changes in NO_x can be largely attributed to limited shift in low- and high-NO_x regimes, to buffering in chemical pathways (e.g., O_3 versus NO_3-initiated oxidation), and to offsetting tendencies in the biogenic versus anthropogenic SOA responses. Our results, based on the global chemistry–climate model CAM4-chem with simplified SOA schemes, indicate that air quality control on anthropogenic NO_x may not have substantial impacts on organic aerosol loadings at large regional scales. Further modeling studies including both process-based and parameterized schemes need to be done to carefully examine the NO_x impact on SOA formation.

The Supplement related to this article is available online at doi:10.5194/acp-15-13487-2015-supplement.

Acknowledgements. Funding support for this study is provided by Yale University, by the National Center for Atmospheric Research, which is operated by the University Corporation for Atmospheric Research on behalf of the National Science Foundation, and by the DOE grant DE-SC0006711 (Alma Hodzic, Christoph Knote). Computing resources are provided by the Climate Simulation Laboratory at NCAR's Computational and Information Systems Laboratory (CISL), sponsored by the National Science Foundation and other agencies.

Disclaimer. Any opinions, findings and conclusions or recommendations expressed in the publication are those of the author(s) and do not necessarily reflect the views of the National Science Foundation.

Edited by: D. Farmer

References

Ahmadov, R., McKeen, S. A., Robinson, A. L., Bahreini, R., Middlebrook, A. M., de Gouw, J. A., Meagher, J., Hsie, E.-Y., Edgerton, E., Shaw, S., and Trainer, M.: A volatility basis set model for summertime secondary organic aerosols over the Eastern United States in 2006, J. Geophys. Res., 117, 1–19, doi:10.1029/2011JD016831, 2012.

Aiken, A. C., Decarlo, P. F., Kroll, J. H., Worsnop, D. R., Huffman, J. A., Docherty, K. S., Ulbrich, I. M., Mohr, C., Kimmel, J. R., Sueper, D., Sun, Y., Zhang, Q., Trimborn, A., Northway, M., Ziemann, P. J., Canagaratna, M. R., Onasch, T. B., Alfarra, M. R., Prevot, A. S. H., Dommen, J., Duplissy, J., Metzger, A., Baltensperger, U., and Jimenez, J. L.: O/C and OM/OC ratios of primary, secondary, and ambient organic aerosols with high-resolution time-of-flight aerosol mass spectrometry, Environ. Sci. Technol., 42, 4478–4485, doi:10.1021/es703009q, 2008.

Aiken, A. C., Salcedo, D., Cubison, M. J., Huffman, J. A., DeCarlo, P. F., Ulbrich, I. M., Docherty, K. S., Sueper, D., Kimmel, J. R., Worsnop, D. R., Trimborn, A., Northway, M., Stone, E. A., Schauer, J. J., Volkamer, R. M., Fortner, E., de Foy, B., Wang, J., Laskin, A., Shutthanandan, V., Zheng, J., Zhang, R., Gaffney, J., Marley, N. A., Paredes-Miranda, G., Arnott, W. P., Molina, L. T., Sosa, G., and Jimenez, J. L.: Mexico City aerosol analysis during MILAGRO using high resolution aerosol mass spectrometry at the urban supersite (T0) – Part 1: Fine particle composition and organic source apportionment, Atmos. Chem. Phys., 9, 6633–6653, doi:10.5194/acp-9-6633-2009, 2009.

Andreae, M. O. and Crutzen, P. J.: Atmospheric Aerosols: Biogeochemical Sources and Role in Atmospheric Chemistry, Science, 276, 1052–1058, doi:10.1126/science.276.5315.1052, 1997.

Athanasopoulou, E., Vogel, H., Vogel, B., Tsimpidi, A. P., Pandis, S. N., Knote, C., and Fountoukis, C.: Modeling the meteorological and chemical effects of secondary organic aerosols during an EUCAARI campaign, Atmos. Chem. Phys., 13, 625–645, doi:10.5194/acp-13-625-2013, 2013.

Atkinson, R. and Arey, J.: Atmospheric Degradation of Volatile Organic Compounds Atmospheric Degradation of Volatile Organic Compounds, Chem. Rev., 103, 4605–4638, doi:10.1021/cr0206420, 2003.

Barth, M. C., Rasch, P. J., Kiehl, J. T., Benkovitz, C. M., and Schwartz, S. E.: Sulfur chemistry in the National Center for Atmospheric Research Community Climate Model: Description, evaluation, features, and sensitivity to aqueous chemistry, J. Geophys. Res., 105, 1387, doi:10.1029/1999JD900773, 2000.

Canagaratna, M. R., Jayne, J. T., Jimenez, J. L., Allan, J. D., Alfarra, M. R., Zhang, Q., Onasch, T. B., Drewnick, F., Coe, H., Middlebrook, A., Delia, A., Williams, L. R., Trimborn, A. M., Northway, M. J., DeCarlo, P. F., Kolb, C. E., Davidovits, P., and Worsnop, D. R.: Chemical and microphysical characterization of ambient aerosols with the aerodyne aerosol mass spectrometer, Mass Spectrom. Rev., 26, 185–222, doi:10.1002/mas.20115, 2007.

Carlton, A. G., Pinder, R. W., Bhave, P. V., and Pouliot, G. A.: To what extent can biogenic SOA be controlled?, Environ. Sci. Technol., 44, 3376–3380, doi:10.1021/es903506b, 2010.

Carslaw, K. S., Boucher, O., Spracklen, D. V., Mann, G. W., Rae, J. G. L., Woodward, S., and Kulmala, M.: A review of natural aerosol interactions and feedbacks within the Earth system, Atmos. Chem. Phys., 10, 1701–1737, doi:10.5194/acp-10-1701-2010, 2010.

Chen, Q., Liu, Y., Donahue, N. M., Shilling, J. E., and Martin, S. T.: Particle-phase chemistry of secondary organic material: Modeled compared to measured O : C and H:C Elemental ratios provide constraints, Environ. Sci. Technol., 45, 4763–4770, doi:10.1021/es104398s, 2011.

Chow, J. C., Watson, J. G., Pritchett, L. C., Pierson, W. R., Frazier, C. A., and Purcell, R. G.: The dri thermal/optical reflectance carbon analysis system: description, evaluation and applications in U.S. Air quality studies, Atmos. Environ. Part A. Gen. Top., 27, 1185–1201, doi:10.1016/0960-1686(93)90245-T, 1993.

Dillner, A. M., Phuah, C. H., and Turner, J. R.: Effects of post-sampling conditions on ambient carbon aerosol filter measurements, Atmos. Environ., 43, 5937–5943, doi:10.1016/j.atmosenv.2009.08.009, 2009.

Donahue, N. M., Robinson, A. L., Stanier, C. O., and Pandis, S. N.: Coupled partitioning, dilution, and chemical aging of semivolatile organics, Environ. Sci. Technol., 40, 2635–2643, doi:10.1021/es052297c, 2006.

Emanuelsson, E. U., Hallquist, M., Kristensen, K., Glasius, M., Bohn, B., Fuchs, H., Kammer, B., Kiendler-Scharr, A., Nehr, S., Rubach, F., Tillmann, R., Wahner, A., Wu, H.-C., and Mentel, Th. F.: Formation of anthropogenic secondary organic aerosol (SOA) and its influence on biogenic SOA properties, Atmos. Chem. Phys., 13, 2837–2855, doi:10.5194/acp-13-2837-2013, 2013.

Frost, G. J., McKeen, S. A., Trainer, M., Ryerson, T. B., Neuman, J. A., Roberts, J. M., Swanson, A., Holloway, J. S., Sueper, D. T., Fortin, T., Parrish, D. D., Fehsenfeld, F. C., Flocke, F., Peckham, S. E., Grell, G. A., Kowal, D., Cartwright, J., Auerbach, N., and Habermann, T.: Effects of changing power plant NOx emissions on ozone in the eastern United States: Proof of concept, J. Geophys. Res., 111, D12306, doi:10.1029/2005jd006354, 2006.

Granier, C., Guenther, A., Lamarque, J. F., Mieville, A., Muller, J., Oliver, J., Orlando, J., Peters, J., Petron, G., Tyndall, G. K., and Wallens, S.: POET, a database of surface emissions of ozone precursors, available at: http://www.aero.jussieu.fr/projet/ACCENT/POET.php (last access: August 2008), 2005.

Griffin, R. J., Cocker, D. R., Seinfeld, J. H., and Dabdub, D.: Estimate of global atmospheric organic aerosol from oxidation of biogenic hydrocarbons, Geophys. Res. Lett., 26, 2721, doi:10.1029/1999GL900476, 1999.

Guenther, A. B., Karl, T., Harley, P., Wiedinmyer, C., Palmer, P. I. and Geron, C.: Estimates of global terrestrial isoprene emissions using MEGAN (Model of Emissions of Gases and Aerosols from Nature), Atmos. Chem. Phys., 6, 3181–3210, doi:10.5194/acp-6-3181-2006, 2006.

Guenther, A. B., Jiang, X., Heald, C. L., Sakulyanontvittaya, T., Duhl, T., Emmons, L. K., and Wang, X.: The Model of Emissions of Gases and Aerosols from Nature version 2.1 (MEGAN2.1): an extended and updated framework for modeling biogenic emissions, Geosci. Model Dev., 5, 1471–1492, doi:10.5194/gmd-5-1471-2012, 2012.

Hand, J. L., Copeland, S. A., Day, D. E., Dillner, A. M., Indresand, H., Malm, W. C., McDade, C. E., Moore, C. T., Pitchford, M. L., Schichtel, B. A., and Watson, J. G.: Spatial and Seasonal Patterns and Temporal Variability of Haze and its Constituents in the United States Report V, June 2011.

Heald, C. L., Henze, D. K., Horowitz, L. W., Feddema, J., Lamarque, J. F., Guenther, A., Hess, P. G., Vitt, F., Seinfeld, J. H., Godstein, A. H., and Fung, I.: Predicted change in global secondary organic aerosol concentrations in response to future climate, emissions, and land use change, J. Geophys. Res. Atmos., 113, 1–16, doi:10.1029/2007JD009092, 2008.

Heald, C. L., Kroll, J. H., Jimenez, J. L., Docherty, K. S., Decarlo, P. F., Aiken, A. C., Chen, Q., Martin, S. T., Farmer, D. K., and Artaxo, P.: A simplified description of the evolution of organic aerosol composition in the atmosphere, Geophys. Res. Lett., 37, L08803, doi:10.1029/2010GL042737, 2010.

Heald, C. L., Coe, H., Jimenez, J. L., Weber, R. J., Bahreini, R., Middlebrook, A. M., Russell, L. M., Jolleys, M., Fu, T.-M., Allan, J. D., Bower, K. N., Capes, G., Crosier, J., Morgan, W. T., Robinson, N. H., Williams, P. I., Cubison, M. J., DeCarlo, P. F., and Dunlea, E. J.: Exploring the vertical profile of atmospheric organic aerosol: comparing 17 aircraft field campaigns with a global model, Atmos. Chem. Phys., 11, 12673–12696, doi:10.5194/acp-11-12673-2011, 2011.

Hodzic, A. and Jimenez, J. L.: Modeling anthropogenically controlled secondary organic aerosols in a megacity: a simplified framework for global and climate models, Geosci. Model Dev., 4, 901–917, doi:10.5194/gmd-4-901-2011, 2011.

Hodzic, A., Madronich, S., Kasibhatla, P. S., Tyndall, G., Aumont, B., Jimenez, J. L., Lee-Taylor, J., and Orlando, J.: Organic photolysis reactions in tropospheric aerosols: effect on secondary organic aerosol formation and lifetime, Atmos. Chem. Phys., 15, 9253–9269, doi:10.5194/acp-15-9253-2015, 2015.

Hoyle, C. R., Boy, M., Donahue, N. M., Fry, J. L., Glasius, M., Guenther, A., Hallar, A. G., Huff Hartz, K., Petters, M. D., Petäjä, T., Rosenoern, T., and Sullivan, A. P.: A review of the anthropogenic influence on biogenic secondary organic aerosol, Atmos. Chem. Phys., 11, 321–343, doi:10.5194/acp-11-321-2011, 2011.

Hu, W. W., Hu, M., Yuan, B., Jimenez, J. L., Tang, Q., Peng, J. F., Hu, W., Shao, M., Wang, M., Zeng, L. M., Wu, Y. S., Gong, Z. H., Huang, X. F., and He, L. Y.: Insights on organic aerosol aging and the influence of coal combustion at a regional receptor site of central eastern China, Atmos. Chem. Phys., 13, 10095–10112, doi:10.5194/acp-13-10095-2013, 2013.

Huang, R.-J., Zhang, Y., Bozzetti, C., Ho, K.-F., Cao, J.-J., Han, Y., Daellenbach, K. R., Slowik, J. G., Platt, S. M., Canonaco, F., Zotter, P., Wolf, R., Pieber, S. M., Bruns, E. A., Crippa, M., Ciarelli, G., Piazzalunga, A., Schwikowski, M., Abbaszade, G., Schnelle-Kreis, J., Zimmermann, R., An, Z., Szidat, S., Baltensperger, U., Haddad, I. El, and Prévôt, A. S. H.: High secondary aerosol contribution to particulate pollution during haze events in China, Nature, 514, 218–222, doi:10.1038/nature13774, 2014.

Kanakidou, M., Seinfeld, J. H., Pandis, S. N., Barnes, I., Dentener, F. J., Facchini, M. C., Van Dingenen, R., Ervens, B., Nenes, A., Nielsen, C. J., Swietlicki, E., Putaud, J. P., Balkanski, Y., Fuzzi, S., Horth, J., Moortgat, G. K., Winterhalter, R., Myhre, C. E. L., Tsigaridis, K., Vignati, E., Stephanou, E. G. and Wilson, J.: Organic aerosol and global climate modelling: a review, Atmos. Chem. Phys., 5, 1053–1123, doi:10.5194/acp-5-1053-2005, 2005.

Kim, S. W., Heckel, A., McKeen, S. A., Frost, G. J., Hsie, E. Y., Trainer, M. K., Richter, A., Burrows, J. P., Peckham, S. E., and Grell, G. A.: Satellite-observed U.S. power plant NOx emission reductions and their impact on air quality, Geophys. Res. Lett., 33, L22812, doi:10.1029/2006GL027749, 2006.

Knote, C., Hodzic, A., and Jimenez, J. L.: The effect of dry and wet deposition of condensable vapors on secondary organic aerosols concentrations over the continental US, Atmos. Chem. Phys., 15, 1–18, doi:10.5194/acp-15-1-2015, 2015.

Kroll, J. H. and Seinfeld, J. H.: Chemistry of secondary organic aerosol: Formation and evolution of low-volatility organics in the atmosphere, Atmos. Environ., 42, 3593–3624, doi:10.1016/j.atmosenv.2008.01.003, 2008.

Kroll, J. H., Ng, N. L., Murphy, S. M., Flagan, R. C., and Seinfeld, J. H.: Secondary organic aerosol formation from isoprene photooxidation, Environ. Sci. Technol., 40, 1869–1877, doi:10.1021/es0524301, 2006.

Lamarque, J.-F., Emmons, L. K., Hess, P. G., Kinnison, D. E., Tilmes, S., Vitt, F., Heald, C. L., Holland, E. A., Lauritzen, P. H., Neu, J., Orlando, J. J., Rasch, P. J., and Tyndall, G. K.: CAM-chem: description and evaluation of interactive at-

mospheric chemistry in the Community Earth System Model, Geosci. Model Dev., 5, 369–411, doi:10.5194/gmd-5-369-2012, 2012.

Lane, T. E., Donahue, N. M., and Pandis, S. N.: Simulating secondary organic aerosol formation using the volatility basis-set approach in a chemical transport model, Atmos. Environ., 42, 7439–7451, doi:10.1016/j.atmosenv.2008.06.026, 2008.

Lanz, V. A., Alfarra, M. R., Baltensperger, U., Buchmann, B., Hueglin, C., and Prévôt, A. S. H.: Source apportionment of submicron organic aerosols at an urban site by factor analytical modelling of aerosol mass spectra, Atmos. Chem. Phys., 7, 1503–1522, doi:10.5194/acp-7-1503-2007, 2007.

Lee-Taylor, J., Hodzic, A., Madronich, S., Aumont, B., Camredon, M., and Valorso, R.: Multiday production of condensing organic aerosol mass in urban and forest outflow, Atmos. Chem. Phys., 15, 595–615, doi:10.5194/acp-15-595-2015, 2015.

Lin, Y.-H., Knipping, E. M., Edgerton, E. S., Shaw, S. L., and Surratt, J. D.: Investigating the influences of SO_2 and NH_3 levels on isoprene-derived secondary organic aerosol formation using conditional sampling approaches, Atmos. Chem. Phys., 13, 8457–8470, doi:10.5194/acp-13-8457-2013, 2013.

Ng, N. L., Kroll, J. H., Chan, A. W. H., Chhabra, P. S., Flagan, R. C., and Seinfeld, J. H.: Secondary organic aerosol formation from m-xylene, toluene, and benzene, Atmos. Chem. Phys., 7, 3909–3922, doi:10.5194/acp-7-3909-2007, 2007.

Ng, N. L., Kwan, A. J., Surratt, J. D., Chan, A. W. H., Chhabra, P. S., Sorooshian, A., Pye, H. O. T., Crounse, J. D., Wennberg, P. O., Flagan, R. C., and Seinfeld, J. H.: Secondary organic aerosol (SOA) formation from reaction of isoprene with nitrate radicals (NO_3), Atmos. Chem. Phys., 8, 4117–4140, doi:10.5194/acp-8-4117-2008, 2008.

Odum, J. R., Hoffmann, T., Bowman, F., Collins, D., Flagan, R. C., and Seinfeld, J. H.: Gas particle partitioning and secondary organic aerosol yields, Environ. Sci. Technol., 30, 2580–2585, doi:10.1021/es950943+, 1996.

Ohara, T., Akimoto, H., Kurokawa, J., Horii, N., Yamaji, K., Yan, X., and Hayasaka, T.: An Asian emission inventory of anthropogenic emission sources for the period 1980–2020, Atmos. Chem. Phys., 7, 4419–4444, doi:10.5194/acp-7-4419-2007, 2007.

Pankow, J. F.: An Absorption-Model of the Gas Aerosol Partitioning Involved in the Formation of Secondary Organic Aerosol, Atmos. Environ., 28, 189–193, doi:10.1016/j.atmosenv.2007.10.060, 1994.

Presto, A. A., Huff Hartz, K. E., and Donahue, N. M.: Secondary organic aerosol production from terpene ozonolysis. 2. Effect of NOx concentration, Environ. Sci. Technol., 39, 7046–7054, doi:10.1021/es050400s, 2005.

Putaud, J. P., Van Dingenen, R., Alastuey, A., Bauer, H., Birmili, W., Cyrys, J., Flentje, H., Fuzzi, S., Gehrig, R., Hansson, H. C., Harrison, R. M., Herrmann, H., Hitzenberger, R., Hüglin, C., Jones, A. M., Kasper-Giebl, A., Kiss, G., Kousa, A., Kuhlbusch, T. A. J., Löschau, G., Maenhaut, W., Molnar, A., Moreno, T., Pekkanen, J., Perrino, C., Pitz, M., Puxbaum, H., Querol, X., Rodriguez, S., Salma, I., Schwarz, J., Smolik, J., Schneider, J., Spindler, G., ten Brink, H., Tursic, J., Viana, M., Wiedensohler, A., and Raes, F.: A European aerosol phenomenology – 3: Physical and chemical characteristics of particulate matter from 60 rural, urban, and kerbside sites across Europe, Atmos. Environ., 44, 1308–1320, doi:10.1016/j.atmosenv.2009.12.011, 2010.

Pye, H. O. T., Chan, A. W. H., Barkley, M. P., and Seinfeld, J. H.: Global modeling of organic aerosol: the importance of reactive nitrogen (NO_x and NO_3), Atmos. Chem. Phys., 10, 11261–11276, doi:10.5194/acp-10-11261-2010, 2010.

Robinson, A. L., Donahue, N. M., Shrivastava, M. K., Weitkamp, E. A., Sage, A. M., Grieshop, A. P., Lane, T. E., Pierce, J. R., and Pandis, S. N.: Rethinking Organic Aerosols: Semivolatile Emissions and Photochemical Aging, Science, 80, 1259–1262, doi:10.1126/science.1133061, 2007.

Rollins, A. W., Browne, E. C., Pusede, S. E., Wooldridge, P. J., Gentner, D. R., Goldstein, A. H., Liu, S., Day, D. A., and Cohen, R. C.: Evidence for NOx Control over Nighttime SOA formation, Science, 337, 1210–1212, doi:10.1126/science.1221520, 2012.

Seinfeld, J. H. and Pandis, S. N.: Atmospheric Chemistry and Physics: From Air Pollution to Climate Change, 2nd Edn., Wiley, New York, USA, 2006.

Seinfeld, J. H. and Pankow, J. F.: Organic atmospheric particulate material, Annu. Rev. Phys. Chem., 54, 121–140, doi:10.1146/annurev.physchem.54.011002.103756, 2003.

Shrivastava, M. K., Lane, T. E., Donahue, N. M., Pandis, S. N., and Robinson, A. L.: Effects of gas particle partitioning and aging of primary emissions on urban and regional organic aerosol concentrations, J. Geophys. Res. Atmos., 113, 1–16, doi:10.1029/2007JD009735, 2008.

Spracklen, D. V., Jimenez, J. L., Carslaw, K. S., Worsnop, D. R., Evans, M. J., Mann, G. W., Zhang, Q., Canagaratna, M. R., Allan, J., Coe, H., McFiggans, G., Rap, A., and Forster, P.: Aerosol mass spectrometer constraint on the global secondary organic aerosol budget, Atmos. Chem. Phys., 11, 12109–12136, doi:10.5194/acp-11-12109-2011, 2011.

Tilmes, S., Lamarque, J.-F., Emmons, L. K., Kinnison, D. E., Ma, P.-L., Liu, X., Ghan, S., Bardeen, C., Arnold, S., Deeter, M., Vitt, F., Ryerson, T., Elkins, J. W., Moore, F., Spackman, J. R., and Val Martin, M.: Description and evaluation of tropospheric chemistry and aerosols in the Community Earth System Model (CESM1.2), Geosci. Model Dev., 8, 1395–1426, doi:10.5194/gmd-8-1395-2015, 2015.

Tsimpidi, A. P., Karydis, V. A., Zavala, M., Lei, W., Molina, L., Ulbrich, I. M., Jimenez, J. L., and Pandis, S. N.: Evaluation of the volatility basis-set approach for the simulation of organic aerosol formation in the Mexico City metropolitan area, Atmos. Chem. Phys., 10, 525–546, doi:10.5194/acp-10-525-2010, 2010.

van der Werf, G. R., Randerson, J. T., Giglio, L., Collatz, G. J., Kasibhatla, P. S., and Arellano Jr., A. F.: Interannual variability in global biomass burning emissions from 1997 to 2004, Atmos. Chem. Phys., 6, 3423–3441, doi:10.5194/acp-6-3423-2006, 2006.

Volkamer, R., Jimenez, J. L., San Martini, F., Dzepina, K., Zhang, Q., Salcedo, D., Molina, L. T., Worsnop, D. R., and Molina, M. J.: Secondary organic aerosol formation from anthropogenic air pollution: Rapid and higher than expected, Geophys. Res. Lett., 33, L17811, doi:10.1029/2006GL026899, 2006.

Watson, J. G., Chow, J. C., Chen, L. W. A., and Frank, N. H.: Methods to assess carbonaceous aerosol sampling artifacts for IMPROVE and other long-term networks., J. Air Waste Manag. Assoc., 59, 898–911, doi:10.3155/1047-3289.59.8.898, 2009.

Wesely, M. L.: Parameterization of surface resistances to gaseous dry deposition in regional-scale numerical models, Atmos. Environ., 41 (SUPPL.), 52–63, doi:10.1016/j.atmosenv.2007.10.058, 1998.

White, W. H. and Roberts, P. T.: On the Nature and Origins of Visibility-Reducing Aerosols in the Los Angeles Air Basin, Atmos. Environ., 11, 803–812, 1977.

Wiedinmyer, C., Akagi, S. K., Yokelson, R. J., Emmons, L. K., Al-Saadi, J. A., Orlando, J. J., and Soja, A. J.: The Fire INventory from NCAR (FINN): a high resolution global model to estimate the emissions from open burning, Geosci. Model Dev., 4, 625–641, doi:10.5194/gmd-4-625-2011, 2011.

Williams, J. and Koppmann, R.: Volatile Organic Compounds in the Atmosphere: An Overview, in: Volatile Organic Compounds in the Atmosphere, edited by: Koppmann, R., Blackwell Publishing Ltd, Oxford, UK, 1–32, 2007.

Zhang, Q., Worsnop, D. R., Canagaratna, M. R., and Jimenez, J. L.: Hydrocarbon-like and oxygenated organic aerosols in Pittsburgh: insights into sources and processes of organic aerosols, Atmos. Chem. Phys., 5, 3289–3311, doi:10.5194/acp-5-3289-2005, 2005.

Zhang, Q., Jimenez, J. L., Canagaratna, M. R., Allan, J. D., Coe, H., Ulbrich, I., Alfarra, M. R., Takami, A., Middlebrook, A. M., Sun, Y. L., Dzepina, K., Dunlea, E., Docherty, K., DeCarlo, P. F., Salcedo, D., Onasch, T., Jayne, J. T., Miyoshi, T., Shimono, A., Hatakeyama, S., Takegawa, N., Kondo, Y., Schneider, J., Drewnick, F., Borrmann, S., Weimer, S., Demerjian, K., Williams, P., Bower, K., Bahreini, R., Cottrell, L., Griffin, R. J., Rautiainen, J., Sun, J. Y., Zhang, Y. M., and Worsnop, D. R.: Ubiquity and dominance of oxygenated species in organic aerosols in anthropogenically-influenced Northern Hemisphere midlatitudes, Geophys. Res. Lett., 34, L13801, doi:10.1029/2007GL029979, 2007.

Zhang, X., Cappa, C. D., Jathar, S. H., McVay, R. C., Ensberg, J. J., Kleeman, M. J., and Seinfeld, J. H.: Influence of vapor wall loss in laboratory chambers on yields of secondary organic aerosol., Proc. Natl. Acad. Sci. USA, 111, 5802–5807, doi:10.1073/pnas.1404727111, 2014.

Ziemann, P. J. and Atkinson, R.: Kinetics, products, and mechanisms of secondary organic aerosol formation, Chem. Soc. Rev., 41, 6582, doi:10.1039/c2cs35122f, 2012.